Submitted to: Psychological Methods
February 26, 2022

Supplementary Materials to *Reliable network inference from unreliable data: A tutorial on latent network modeling using STRAND*

Daniel Redhead[1*], Richard McElreath[1], Cody T. Ross[1]

[1] Department of Human Behaviour, Ecology and Culture
Max Planck Institute for Evolutionary Anthropology, Deutscher Platz 6, 04103 Leipzig, Germany.
*Corresponding author: Daniel Redhead, daniel_redhead@eva.mpg.de

Contents

1. Introduction

We conduct several simulation experiments to validate the performance of our models across a broad array of conditions, and to examine if there are any regions of parameter space where the models behave sub-optimally. To do this, we first generate network data using forward simulations from our stochastic blockmodel, our social relations model, and the combined model, which includes both stochastic blockmodel and social relations model parameters. We then use the corresponding inferential statistical models to analyze the simulated data and ensure that we can recover the generative parameter values. Likewise, to assess the performance of our latent network model, we first simulate 'true' networks of directed ties, and then double-sampled self-reports of these directed ties. These simulated reports are subject to the typical reporting biases outlined in the main text of our manuscript. In each simulation experiment, we generally vary only a single generative parameter (e.g., the false positive rate) across a broad parameter space that contains realistic values, while fixing all other parameters in the model to empirically plausible values.

2. Stochastic Block Model Validation

To begin our model validation procedure, we conduct a simulation experiment in which we generate data using the stochastic blockmodel simulation function provided in `STRAND` and then analyse these data using the corresponding model fitting and inference functions.

Figure 1a shows the predicted in-block and out-block tie rates (shown in yellow), along with the generative parameter values (shown in black), as sample size increases. We successfully recover the parameter values across a wide range of sample sizes; however, the precision of our estimates improves as sample size grows. We repeat this procedure in Figures 1b-1f, varying the generative parameter of interest (e.g., number of observed blocks, within- and between-block tie rates, etc.). Across all of these parameter sweeps, we accurately recover all generative parameter values.

[Fig. 1 about here.]

3. Social Relations Model Validation

To continue our model validation procedure, we conduct a simulation experiment in which we generate data using the social relations model simulation function provided in `STRAND` and then analyse these data using the corresponding model fitting and inference functions.

As with the stochastic blockmodel validation, we begin by demonstrating that our social relations model can accurately recover generative scaler parameters (shown in Figure 2). Then, because the social relations model includes individual- and dyad-level random effects, we also examine whether our model accurately recovers these parameters. To measure the similarity between the generative and estimated parameters, we calculate the correlation coefficient (Figure 3), and the coefficient of normalized mutual information (Figure 4). The correlation coefficient can only detect linear associations between these parameter sets, while the mutual information coefficient can detect non-linear associations. In general, the correlation and mutual information plots both suggest that we reliably recover focal offsets (governing out-degree) and target offsets (governing in-degree). Dyadic offsets are only recoverable in cases where the variance in dyadic random effects is high.

[Fig. 2 about here.]

[Fig. 3 about here.]

[Fig. 4 about here.]

4. Combined Social Relations Model and Stochastic Block Model Validation

The next step of our model validation procedure is to conduct a simulation experiment in which we generate data using the combined stochastic block model and social relations model simulation function provided in `STRAND` and then analyse these data using the corresponding model fitting and inference functions. As with the previous validations, we begin by demonstrating that this model can accurately recover generative scaler parameters (shown in Figure 5). Then, because the social relations model includes individual- and dyad-level random effects, we also examine whether our model accurately recovers these parameters. Similarly, we calculate the correlation coefficient (Figure 6), and the coefficient of normalized mutual information (Figure 7). In general, the correlation and mutual information plots both suggest that we reliably recover focal offsets (governing out-degree) and target offsets (governing in-degree).

[Fig. 5 about here.]

[Fig. 6 about here.]

[Fig. 7 about here.]

5. Latent Network Model Validation

We conducted several simulation experiments to assess the utility of our latent network model across a broad array of conditions, and to examine any underlying features that may affect parameter estimation. To do this, we first simulate a 'true' network of directed ties, and then a double-sampled self-report network of these directed ties that is subject to the typical reporting biases outlined in the main text of our manuscript. In each simulation experiment, we vary only the target of interest (e.g., the false positive rate) across a broad parameter space that contains realistic values, while fixing all other parameters in the model to empirically plausible values. We then evaluate our model's performance across parameter settings—and compare our model to two common network reconstruction approaches, based on use of the union or the intersection of double-sampled ties. We evaluate the similarity of network-level properties (e.g., reciprocity) as calculated from the 'true' network and as calculated from each of the network reconstruction methods. Additionally, we assess the correlation between individual-level network properties (e.g., in-degree) in the true and reconstructed networks.

This section is structured as follows: 1) we first examine our model's ability to recover scalar model parameters, 2) we then assess the ability of our model to accurately capture individual-level parameters (e.g., the recall rate of true ties), 3) we next assess recovery of individual-level network metrics (e.g., in-degree, out-degree, and other centrality measures), and finally, 4) we investigate the model's ability to recover network-level properties (e.g., density, reciprocity, and transitivity). Within each of these sections, we first assess parameter recovery for the most simple case, a base model that accounts for individual-level variation in false positive rates and recall rates of true ties. We then incrementally increase the complexity of our model by incorporating question order biases, attribute-related biases, and finally a third, more accurate 'ground truth' network layer.

5.1. Simple parameter recovery

Here, we investigate the ability of our latent network model to recover the generative parameter values used in our simulation experiments. Across models, we recover nearly all of the parameter values used to generate our true network and our reported networks. This holds across the base model, the question order model, the attribute-related bias model, and the model which integrates ground truth data. Each panel within figures 8–11 represents a separate parameter sweep over the range defined in the sub-figure caption.

As shown in figure 8, there is a slight tendency for our model to underestimate focal-target rho (generalized reciprocity) and dyadic rho (dyadic reciprocity) values. While we adequately capture the recall of true ties across parameters sweeps in figures 8 and 9, we overestimate the recall of true ties for individuals low in an attribute that biases reporting (e.g., status) across parameter sweeps as shown in figure 10 and underestimate the effect that status has on recalling true ties (see figure 4 in the main manuscript). When the same variable affects both true directed ties, and biases reporting on those ties, then the effect of that variable on both outcomes can be difficult—or even impossible—to recover in a statistical model. However, by integrating an additional layer of more accurately observed data, parameter recovery can be achieved as we show in figure 11 here and figure 5 in the main manuscript.

[Fig. 8 about here.]

[Fig. 9 about here.]

[Fig. 10 about here.]

[Fig. 11 about here.]

For the base model, we also investigate edge-wise model accuracy by reporting precision (the sum of true positive classifications divided by the sum of true and false positives), recall (the sum of true positive classifications divided by the sum of true positives and false negatives), and F1 scores (the harmonic mean of precision and recall rates), contrasting our approach with approaches based on the intersection and union of self-reports (figure 12). In the presence of both false positive reports, and failure to recall true ties—e.g., figure 12e—the latent network approach outperforms other methods according to F1 scores.

[Fig. 12 about here.]

5.2. Individual-level parameter recovery

In this section, we examine the ability of our latent network model to accurately recover individual-level parameters. We do this by evaluating the correlation and normalized mutual information between the generative parameters and the recovered parameters. As before, we run these analyses across a broad range of parameter values. Our model generally performs well and recovers individual-level random effect for focal and target offsets (i.e., sender and receiver effects) within the social relations sub-model. However, when the variance across any given array of individual-level random effects is small in the generative model, it becomes increasingly difficult to accurately recover individual-level effects.

[Fig. 13 about here.]

[Fig. 14 about here.]

[Fig. 15 about here.]

[Fig. 16 about here.]

[Fig. 17 about here.]

[Fig. 18 about here.]

[Fig. 19 about here.]

[Fig. 20 about here.]

5.3. Node-level parameter recovery

In this section, we assess the ability of our latent network model to accurately recover node-level parameters. We do this by evaluating the correlation between the node-level quantities calculated on the 'true' network data and the node-level quantities calculated on the reconstructed network data. Networks were reconstructed using our latent network approach, or by using the intersection or union of the reported adjacency matrices. As before, we run these analyses across a broad range of parameter values. Our model performs as well as, or better than, other approaches across almost all parameter sweeps. In some cases, our model performs equivalently to the intersection—however, the intersection only performs well in cases where the recall rate of true ties is near unity. In contrast, our model performs well across a much broader range of settings, and does not require the user to know or assume anything about error rates *a priori*.

[Fig. 21 about here.]

[Fig. 22 about here.]

[Fig. 23 about here.]

[Fig. 24 about here.]

[Fig. 25 about here.]

[Fig. 26 about here.]

[Fig. 27 about here.]

[Fig. 28 about here.]

5.4. Network-level parameter recovery

In this section, we assess the ability of our latent network model to accurately recover several core network-level properties. We do this by calculating network-level measures—i.e., density, reciprocity, transitivity, and measures of centralization—using the 'true' network data and then calculating the same measures using reconstructed network data. Networks were reconstructed using our latent network approach, or by using the intersection or union of the reported networks. As before, we run these analyses across a broad range of parameter values. Our model performs much better than other approaches across almost all parameter sweeps, and nearly always recovers the true network-level values. In contrast, the other approaches diverge substantially from the true values across most parameter sweeps.

[Fig. 29 about here.]

[Fig. 30 about here.]

[Fig. 31 about here.]

[Fig. 32 about here.]

5.5. Recency and frequency parameter recovery

In this section, we assess the ability of our latent network model to accurately recover the flow rates of transfers across true ties in any given time-step. As shown in figure 33, we achieve near-perfect recovery of the generative parameters across all parameter sweeps.

Similarly, in figure 34, we can generally recover the effects that true transfers have on recall of ties. However, in many cases, our model permits recovery only of the average effects of observed transfers on recall. The actual shape of the function linking the recency of observed transfers to recall is not always recoverable.

[Fig. 33 about here.]

[Fig. 34 about here.]

(a) Sample size, $\in (25, \ldots, 350)$

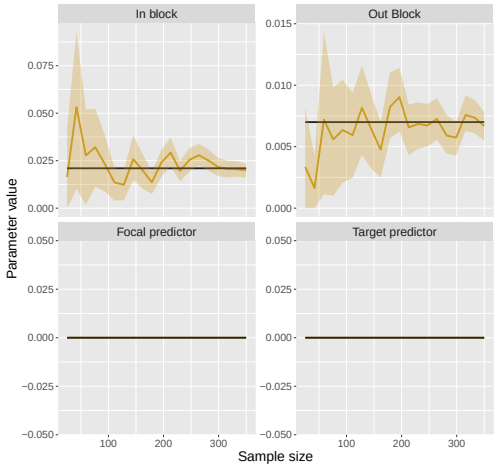

(b) Number of blocks, $\in (1, \ldots, 20)$

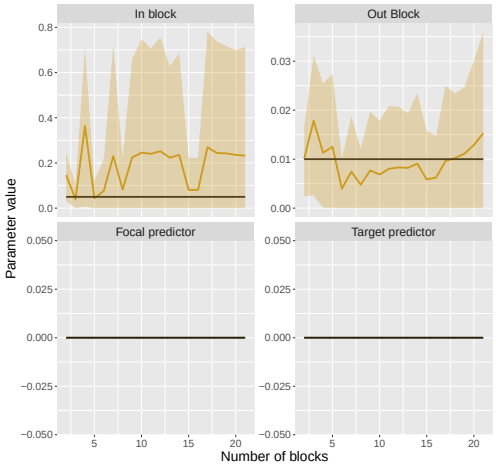

(c) Within-block tie rate, $\in (0.01, \ldots, 0.05)$

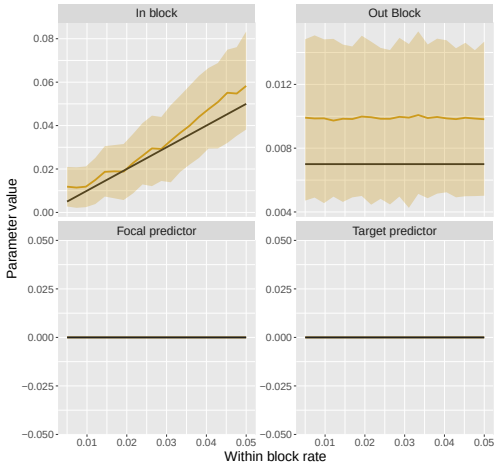

(d) Cross-block tie rate, $\in (0, \ldots, 0.03)$

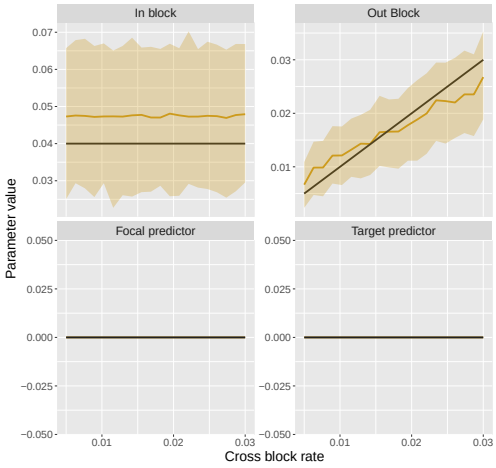

(e) Relative size of block 1 relative to block 2, $\in (0.001, \ldots, 0.80)$

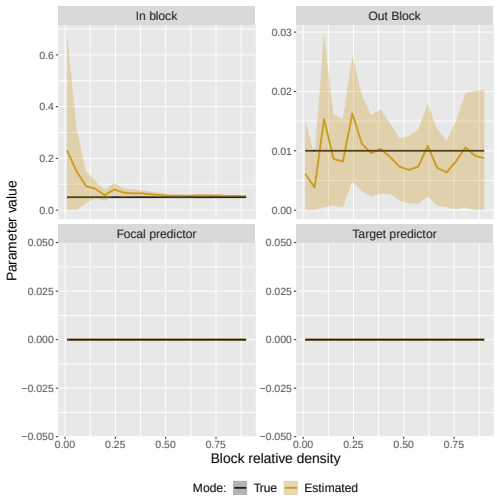

(f) In-degree and out-degree predictor effects, $\in \pm(0, \ldots, 1)$

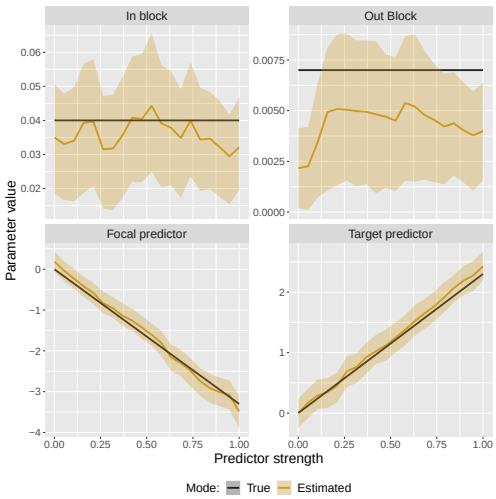

Fig. 1: Parameter recovery from the stochastic block model. Each frame plots the parameter values estimated by our model (in yellow), and the true values specified in the simulation (in black). The y-axis of each sub-figure represents the parameter value, and the x-axis represents the value of the focal simulation parameter given in the sub-heading. For example, the x-axis in figure 1a represents the sample size used when simulating the network data.

(a) Density, $\in (0.001, \ldots, 0.03)$

(b) The effect of a predictor on in-degree and out-degree, $\in (-3, \ldots, 3)$

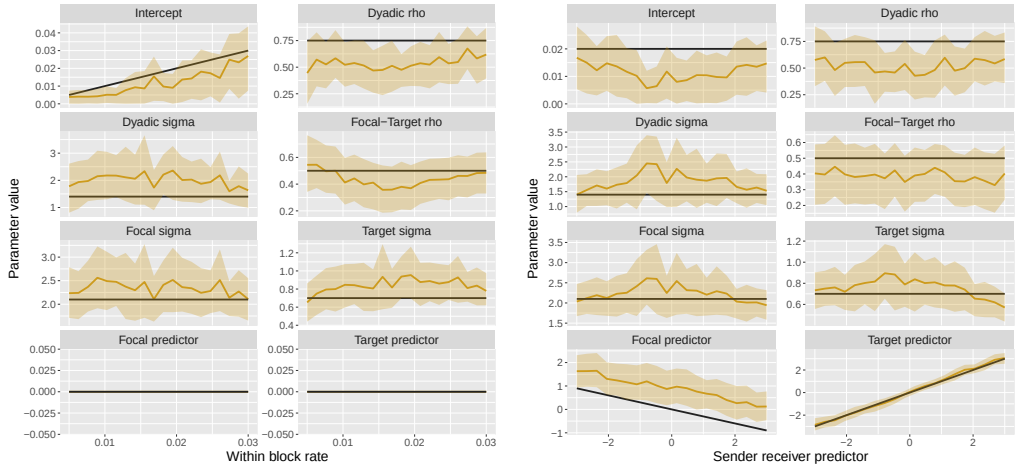

(c) Correlation between in-degree and out-degree, $\in (0.001, \ldots, 0.8)$

(d) SD of in-degree and out-degree, $\in (0.001, \ldots, 5)$

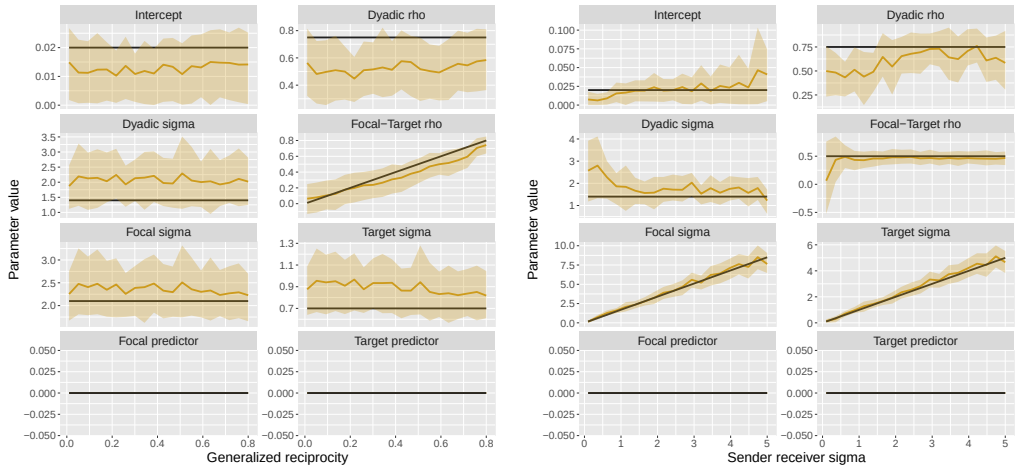

(e) Dyadic reciprocity, $\in (0.001, \ldots, 0.8)$

(f) SD of dyadic random effects, $\in (0.001, \ldots, 5)$

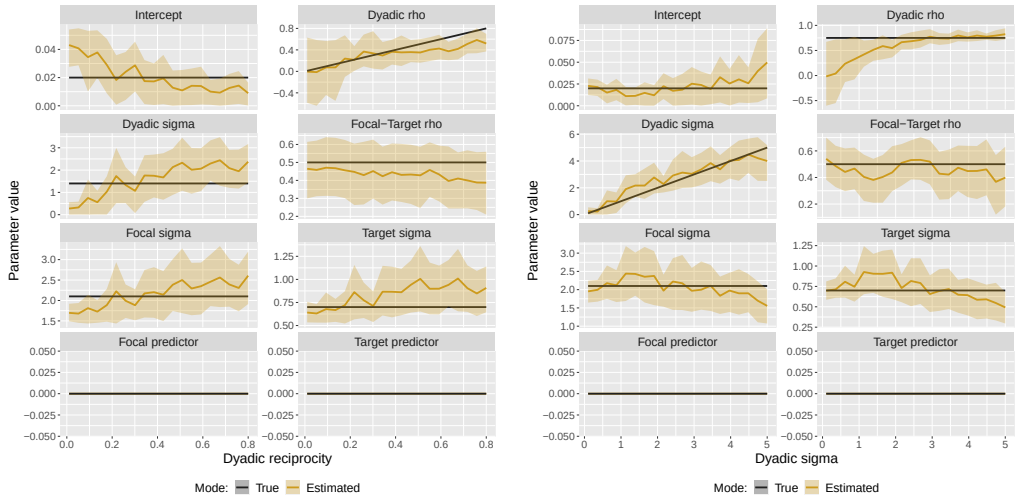

Fig. 2: Parameter recovery from the social relations model. Each frame plots the parameter values estimated by our model (in yellow), and the true values specified in the simulation (in black). The y-axis of each sub-figure represents the parameter value, and the x-axis represents the value of the focal simulation parameter given in the sub-heading. For example, the x-axis in figure 2c represents "generalized reciprocity, or the correlation between sender and receiver random effects, specified when simulating the true network data.

(a) Density, $\in (0.001, \ldots, 0.03)$

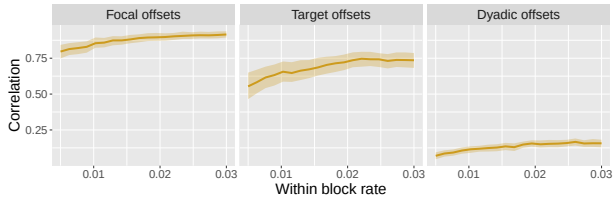

(b) The effect of a predictor on in-degree and out-degree, $\in (-3, \ldots, 3)$

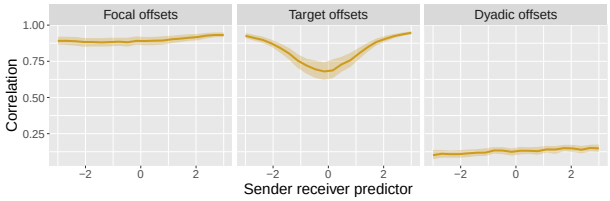

(c) Correlation between in-degree and out-degree, $\in (0.001, \ldots, 0.8)$

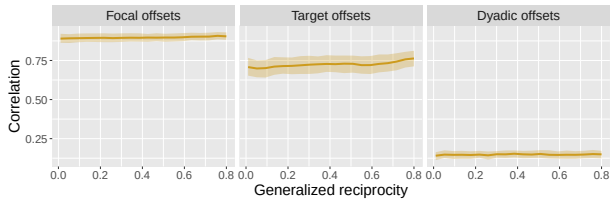

(d) SD of in-degree and out-degree, $\in (0.001, \ldots, 5)$

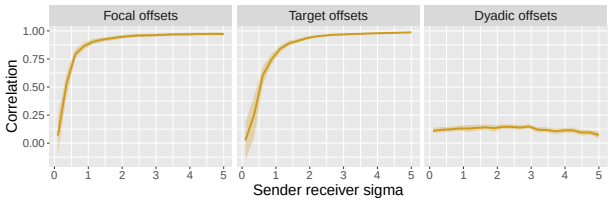

(e) Dyadic reciprocity, $\in (0.001, \ldots, 0.8)$

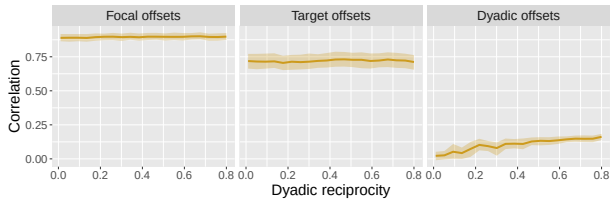

(f) SD of dyadic random effects, $\in (0.001, \ldots, 5)$

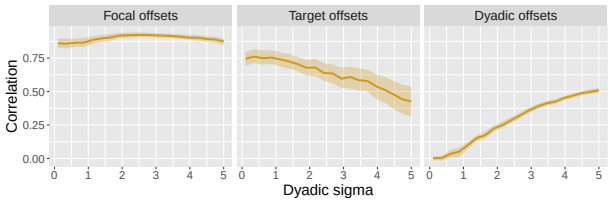

Fig. 3: Individual-level parameter recovery from the social relations model. Each frame plots the correlation between generative parameter values and those estimated by our social relations model. The y-axis of each sub-figure represents the correlation between the generative and estimated parameter values, and the x-axis represents the value of the focal simulation parameter given in the subheading. For example, the x-axis in figure 3e represents the average dyadic reciprocity value used when simulating the network data.

(a) Density, $\in (0.001, \ldots, 0.03)$

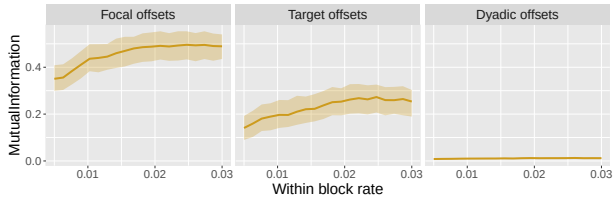

(b) The effect of a predictor on in-degree and out-degree, $\in (-3, \ldots, 3)$

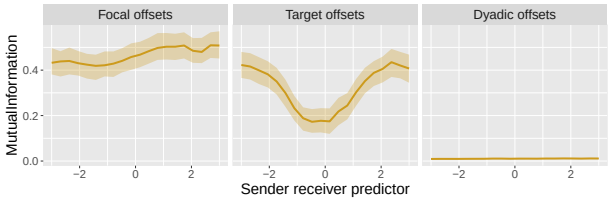

(c) Correlation between in-degree and out-degree, $\in (0.001, \ldots, 0.8)$

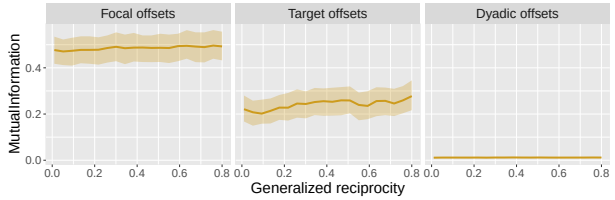

(d) SD of in-degree and out-degree, $\in (0.001, \ldots, 5)$

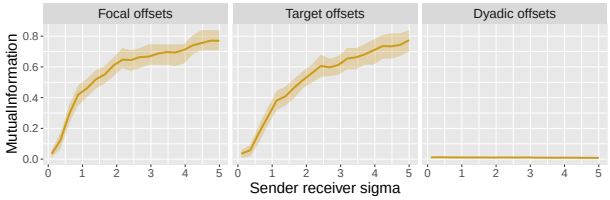

(e) Dyadic reciprocity, $\in (0.001, \ldots, 0.8)$

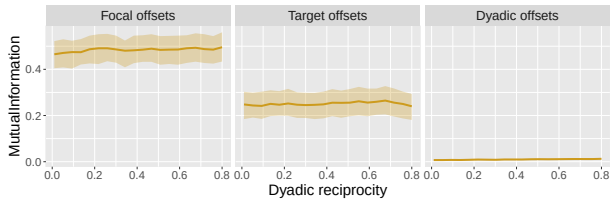

(f) SD of dyadic random effects, $\in (0.001, \ldots, 5)$

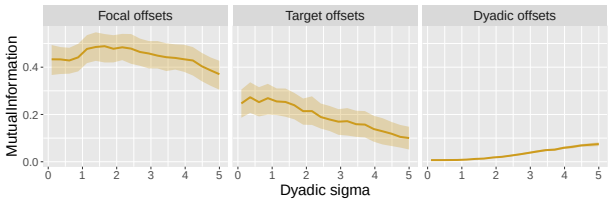

Fig. 4: Individual-level parameter recovery from the social relations model. Each frame plots the mutual information between generative parameter values and those estimated by our social relations model. The y-axis of each sub-figure represents the normalized mutual information between the generative and estimated parameter values, and the x-axis represents the value of the focal simulation parameter given in the subheading. For example, the x-axis in figure 4e represents the average dyadic reciprocity value used when simulating the network data.

(a) In-block tie rate, $\in (0.001, \ldots, 0.05)$

(b) Correlation between in-degree and out-degree, $\in (0.001, \ldots, 0.8)$

(c) SD of in-degree and out-degree, $\in (0.001, \ldots, 5)$

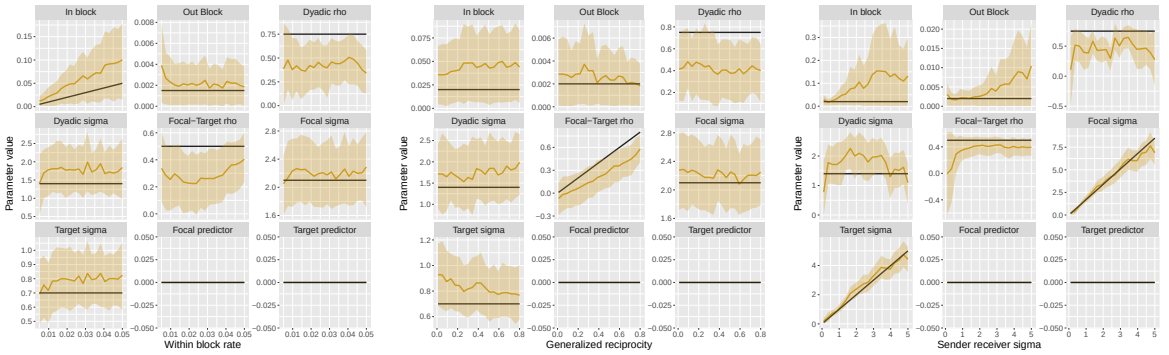

(d) Cross-block ties rate, $\in (0.001, \ldots, 0.01)$

(e) Dyadic reciprocity, $\in (0.001, \ldots, 0.8)$

(f) SD of dyadic random effects, $\in (0.001, \ldots, 5)$

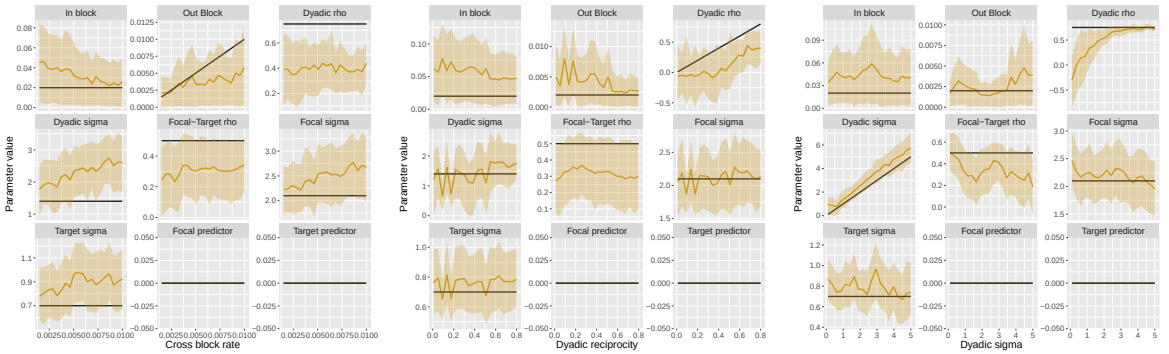

(g) The effect of a predictor on in-degree and out-degree, $\in (-3, \ldots, 3)$

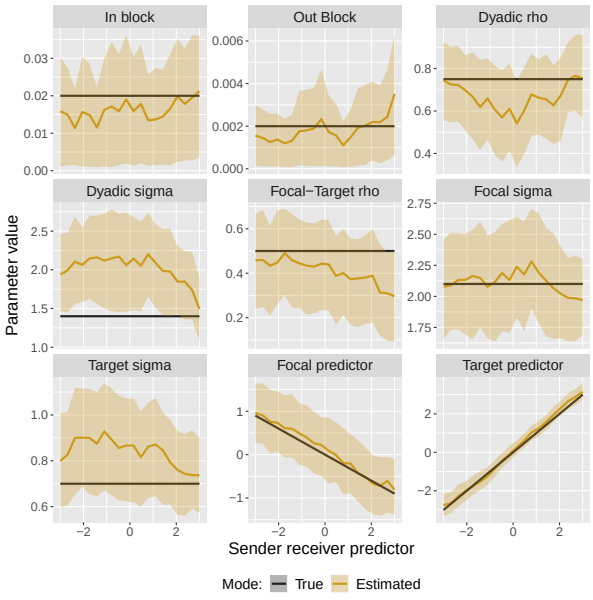

Fig. 5: Parameter recovery from the combined stochastic blockmodel and social relations model. Each frame plots the parameter values estimated by our model (in yellow), and the true values specified in the simulation (in black). The y-axis of each sub-figure represents the parameter value, and the x-axis represents the value of the focal simulation parameter given in the sub-heading. For example, the x-axis in figure 5b represents "generalized reciprocity, or the correlation between sender and receiver random effects, specified when simulating the true network data.

(a) In-block tie rate, $\in (0.001, \ldots, 0.05)$

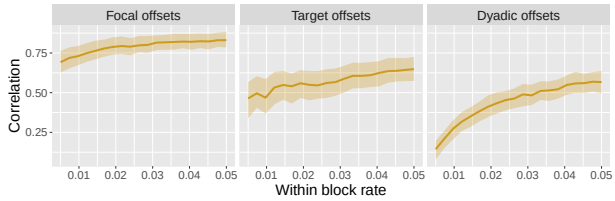

(b) Cross-block ties rate, $\in (0.001, \ldots, 0.01)$

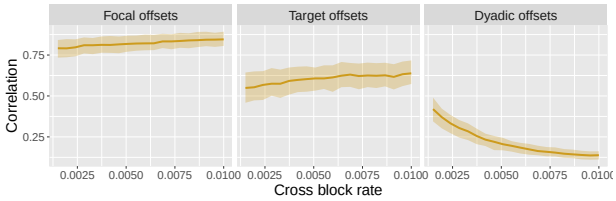

(c) Correlation between in-degree and out-degree, $\in (0.001, \ldots, 0.8)$

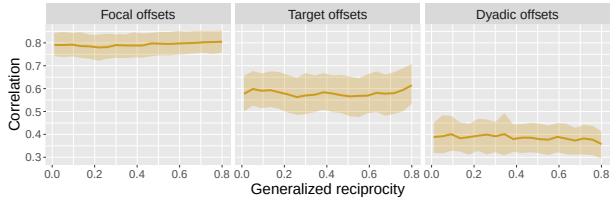

(d) SD of in-degree and out-degree, $\in (0.001, \ldots, 5)$

(e) Dyadic reciprocity, $\in (0.001, \ldots, 0.8)$

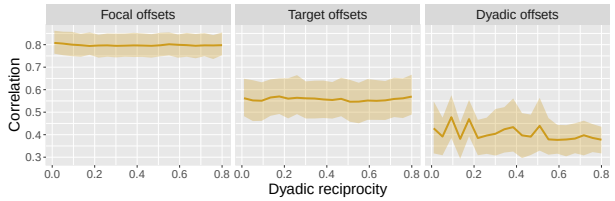

(f) SD of dyadic random effects, $\in (0.001, \ldots, 5)$

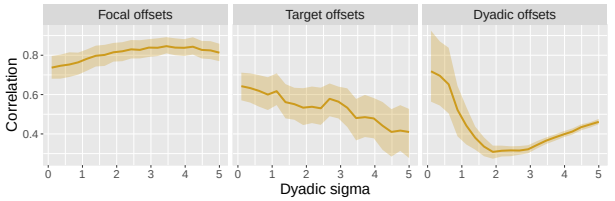

(g) The effect of a predictor on in-degree and out-degree, $\in (-3, \ldots, 3)$

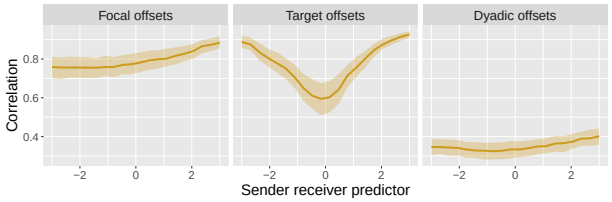

Fig. 6: Individual-level, dyad-level, and block-level parameter recovery from the union of the stochastic block model and the social relations model. Each frame plots the correlation between generative parameter values and those estimated by our joint social relations and stochastic block model. The y-axis of each sub-figure represents the correlation between the generative and estimated parameter values, and the x-axis represents the value of the focal simulation parameter given in the subheading. For example, the x-axis in figure 6c represents "generalized reciprocity, or the correlation between sender and receiver random effects, specified when simulating the reported network data.

(a) In-block tie rate, $\in (0.001, \ldots, 0.05)$

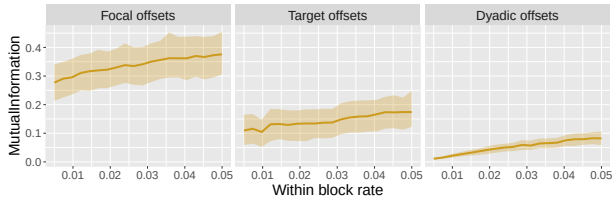

(b) Cross-block ties rate, $\in (0.001, \ldots, 0.01)$

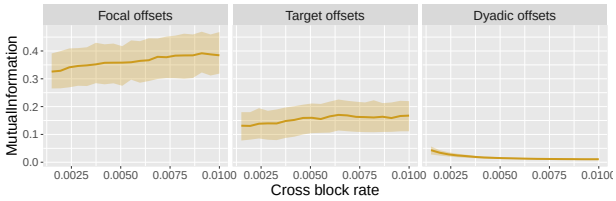

(c) Correlation between in-degree and out-degree, $\in (0.001, \ldots, 0.8)$

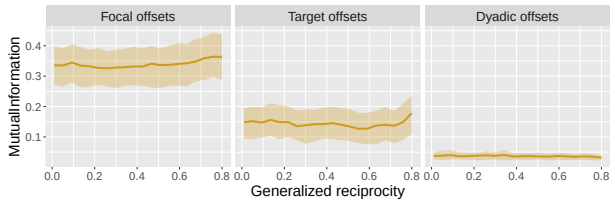

(d) SD of in-degree and out-degree, $\in (0.001, \ldots, 5)$

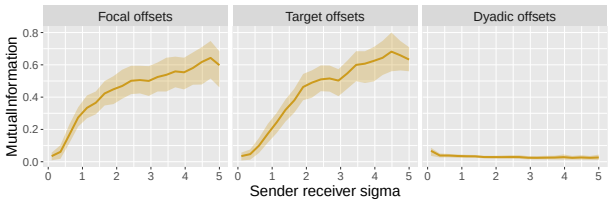

(e) Dyadic reciprocity, $\in (0.001, \ldots, 0.8)$

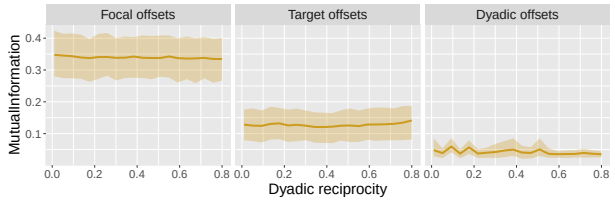

(f) SD of dyadic random effects, $\in (0.001, \ldots, 5)$

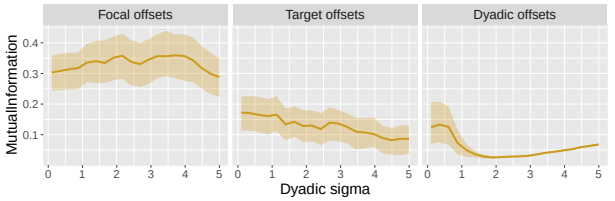

(g) The effect of a predictor on in-degree and out-degree, $\in (-3, \ldots, 3)$

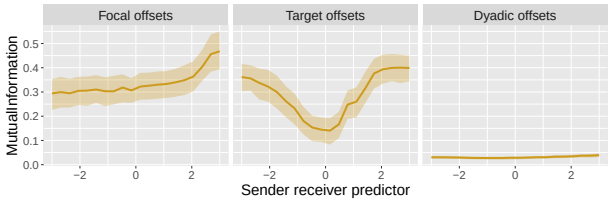

Fig. 7: Individual-level, dyad-level, and block-level parameter recovery from the union of the stochastic block model and the social relations model. Each frame plots the normalized mutual information between generative parameter values and those estimated by our joint social relations and stochastic block model. The y-axis of each sub-figure represents the normalized mutual information between the generative and estimated parameter values, and the x-axis represents the value of the focal simulation parameter given in the subheading. For example, the x-axis in figure 7c represents "generalized" reciprocity, or the correlation between sender and receiver random effects, specified when simulating the reported network data.

(a) Average false positive rate, $\in (0.001, \ldots, 0.05)$

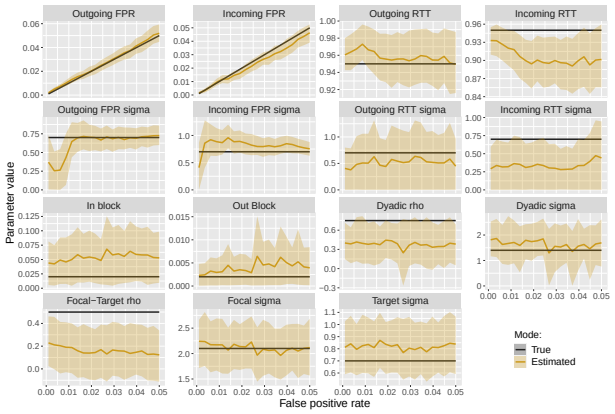

(b) Standard deviation of false positive rate, $\in (0.001, \ldots, 2)$

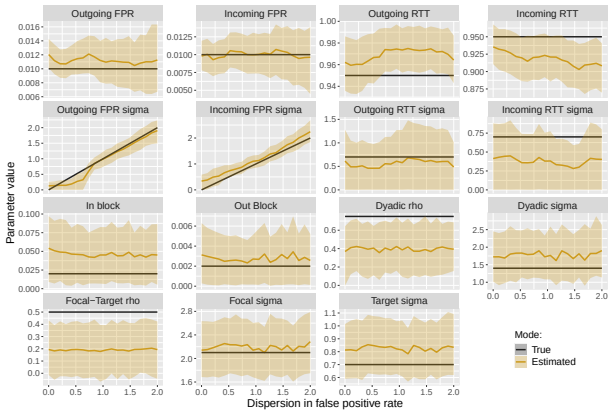

(c) Average recall of true tie rate, $\in (0.4, \ldots, 0.999)$

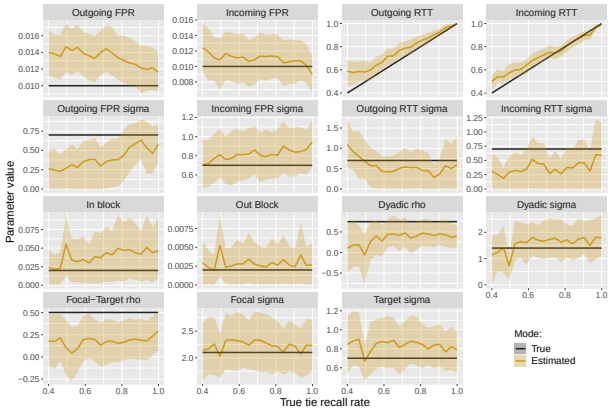

(d) Standard deviation of recall of true tie rate, $\in (0.001, \ldots, 2)$

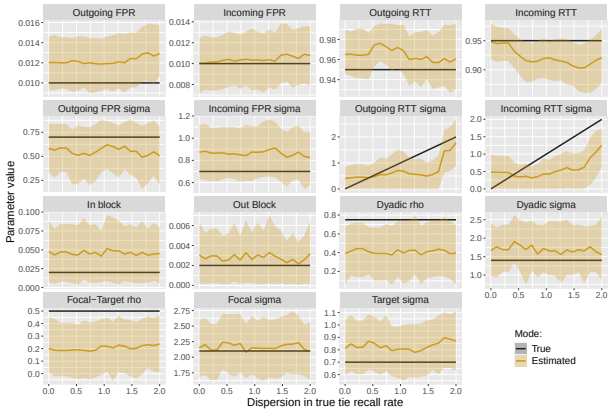

(e) Average false positive rate, $\in (0.001, \ldots, 0.02)$, and average recall of true tie rate, $\in (0.999, \ldots, 0.4)$

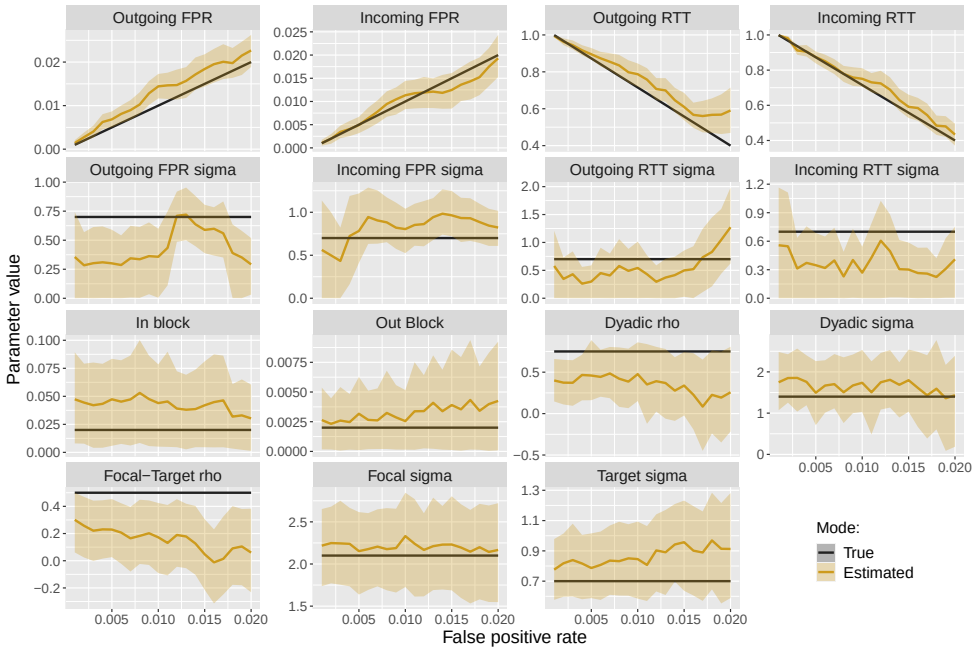

Fig. 8: Parameter recovery from the base model. Each frame plots the parameter values estimated by our latent network model in yellow, and the true values specified in the simulation in black. The y-axis of each sub-figure represents the parameter value, and the x-axis represents the value of the focal simulation parameter given in the subheading. For example, the x-axis in figure 8a represents the average false positive rate used when simulating the reported network data.

(a) Average false positive rate, $\in (0.001, \ldots, 0.05)$

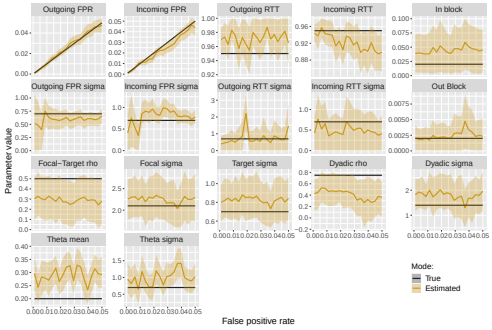

(b) Standard deviation of false positive rate, $\in (0.001, \ldots, 2)$

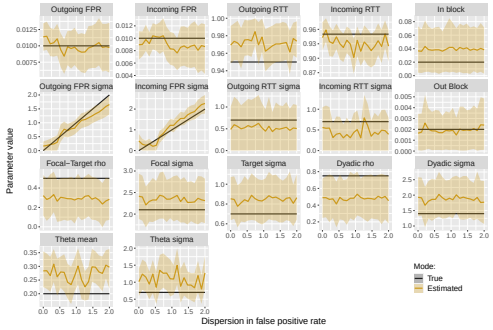

(c) Average recall of true tie rate, $\in (0.4, \ldots, 0.999)$

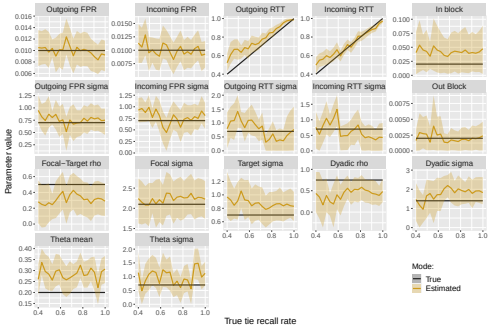

(d) Standard deviation of recall of true tie rate, $\in (0.001, \ldots, 2)$

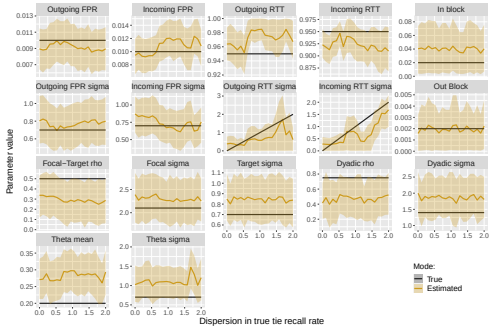

(e) Average recall of true tie rate, $\in (0.4, \ldots, 0.999)$

(f) Standard deviation of recall of true tie rate, $\in (0.001, \ldots, 2)$

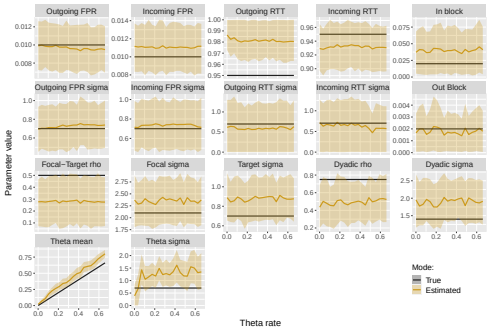

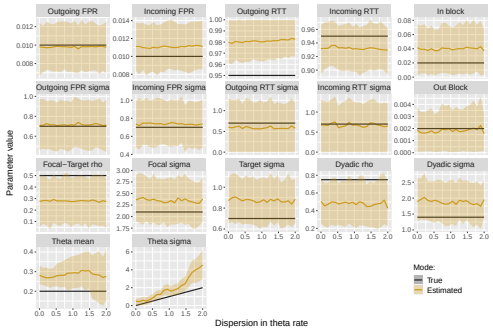

(g) Average false positive rate, $\in (0.001, \ldots, 0.02)$, and average recall of true tie rate, $\in (0.999, \ldots, 0.4)$

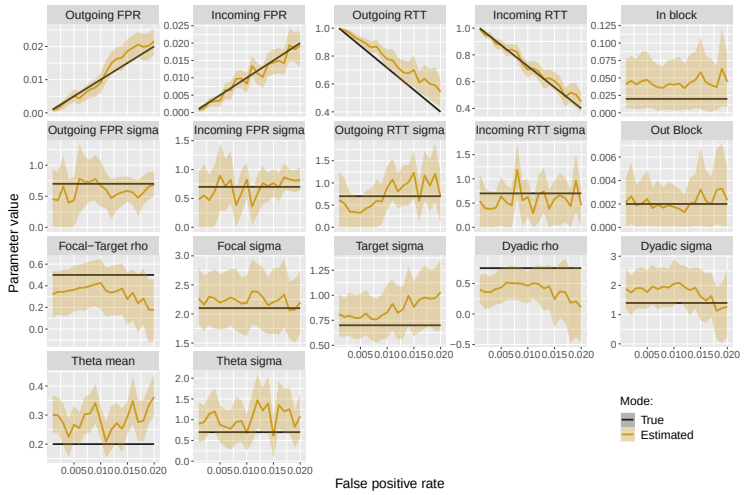

Fig. 9: Parameter recovery from the model incorporating a question-order bias. Each frame plots the parameter values estimated by our latent network model in yellow, and the true values specified in the simulation in black. The y-axis of each sub-figure represents the parameter value, and the x-axis represents the value of the focal simulation parameter given in the subheading. For example, the x-axis in figure 9a represents the average false positive rate used when simulating the reported network data.

(a) Average false positive rate, $\in (0.001, \ldots, 0.05)$

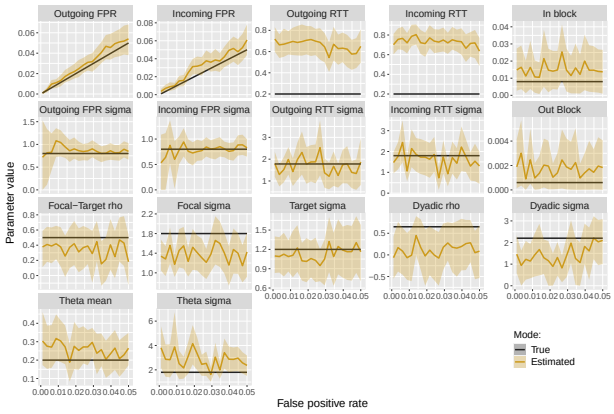

(b) Standard deviation of false positive rate, $\in (0.001, \ldots, 2)$

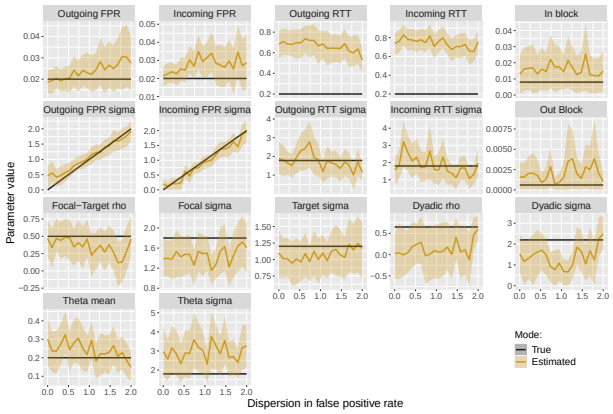

(c) Average recall of true tie rate, $\in (0.4, \ldots, 0.999)$

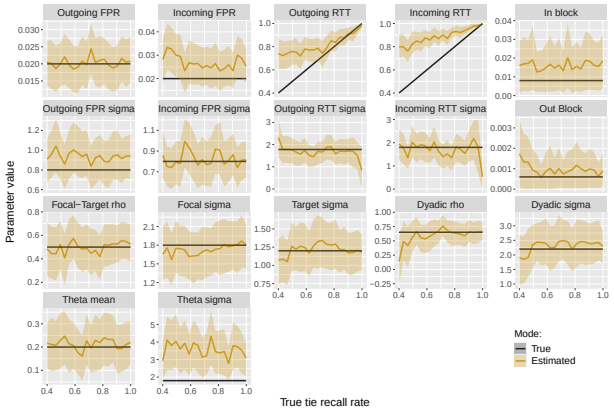

(d) Standard deviation of recall of true tie rate, $\in (0.001, \ldots, 2)$

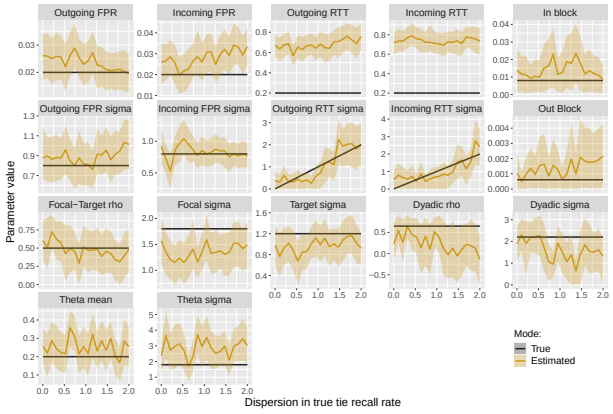

(e) Average false positive rate, $\in (0.001, \ldots, 0.02)$, and average recall of true tie rate, $\in (0.999, \ldots, 0.4)$

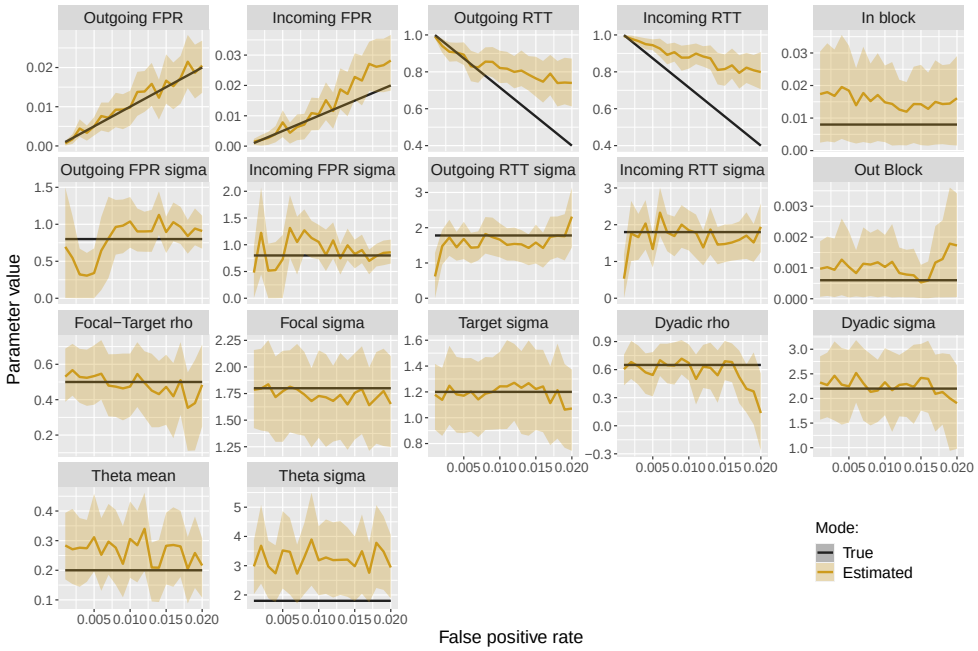

Fig. 10: Parameter recovery from the model incorporating an attribute-related bias. Each frame plots the parameter values estimated by our latent network model in yellow, and the true values specified in the simulation in black. The y-axis of each sub-figure represents the parameter value, and the x-axis represents the value of the focal simulation parameter given in the subheading. For example, the x-axis in figure 10a represents the average false positive rate used when simulating the reported network data.

(a) Average false positive rate, $\in (0.001, \ldots, 0.05)$

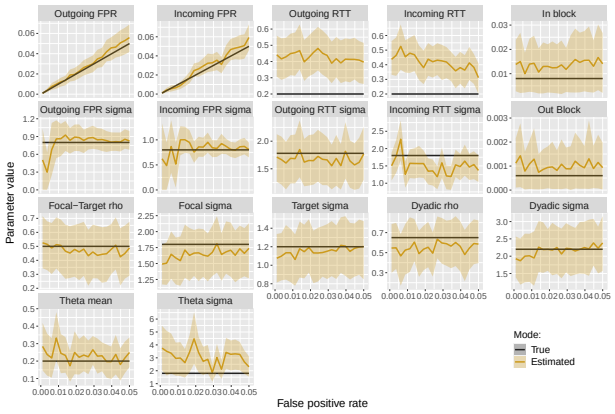

(b) Standard deviation of false positive rate, $\in (0.001, \ldots, 2)$

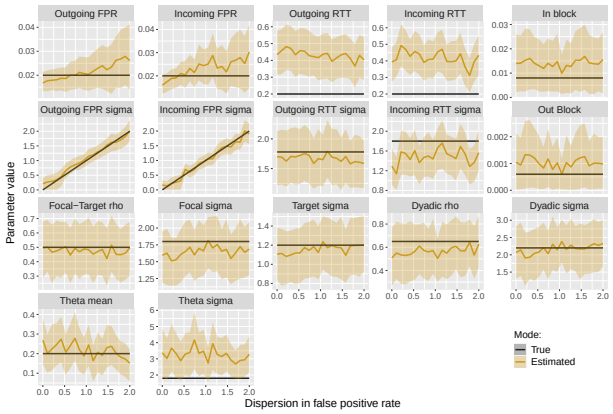

(c) Average recall of true tie rate, $\in (0.4, \ldots, 0.999)$

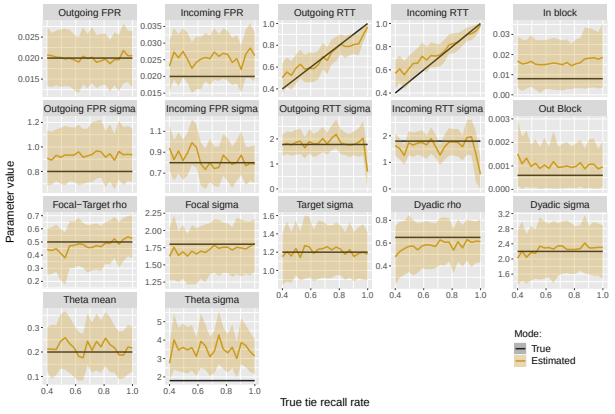

(d) Standard deviation of recall of true tie rate, $\in (0.001, \ldots, 2)$

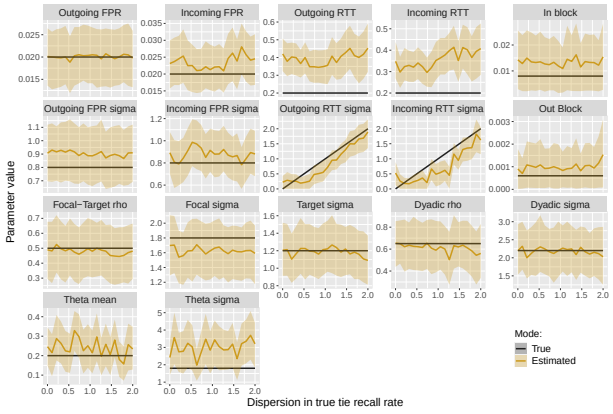

(e) Average false positive rate, $\in (0.001, \ldots, 0.02)$, and average recall of true tie rate, $\in (0.999, \ldots, 0.4)$

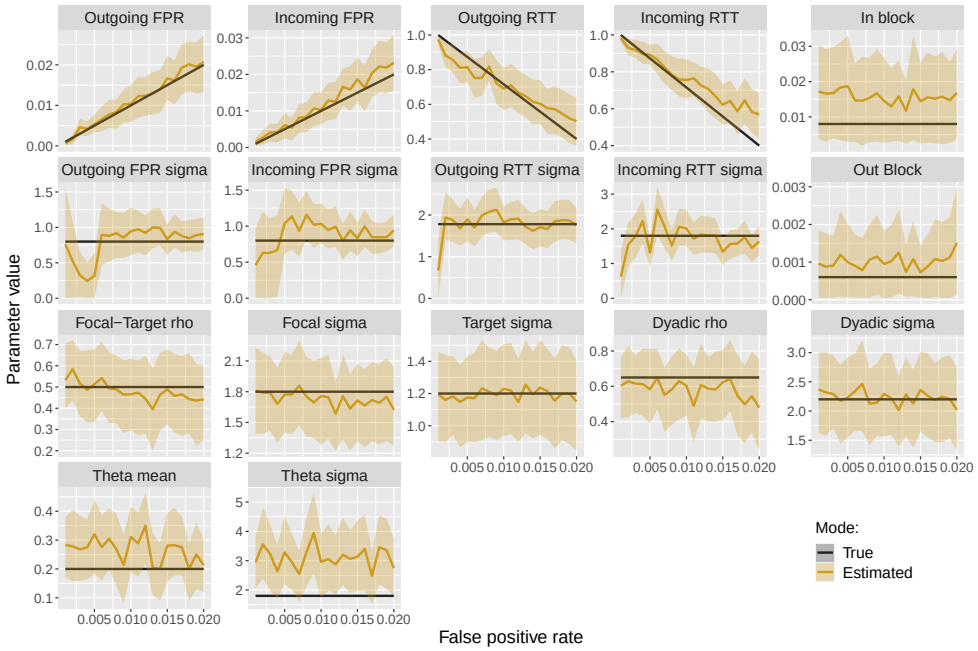

Fig. 11: Parameter recovery from the model incorporating 'ground truth' data. Each frame plots the parameter values estimated by our latent network model in yellow, and the true values specified in the simulation in black. The y-axis of each sub-figure represents the parameter value, and the x-axis represents the value of the focal simulation parameter given in the subheading. For example, the x-axis in figure 11a represents the average false positive rate used when simulating the reported network data.

(a) Average false positive rate, $\in (0.001, \ldots, 0.05)$

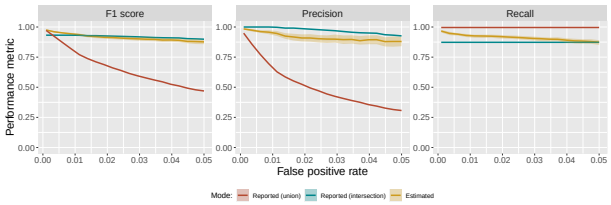

(b) Standard deviation of false positive rate, $\in (0.001, \ldots, 2)$

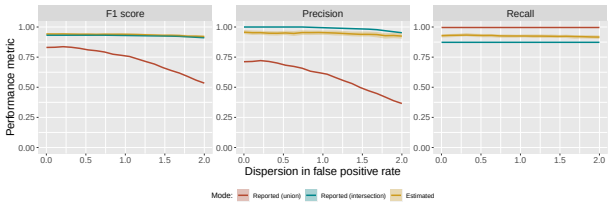

(c) Average recall of true tie rate, $\in (0.4, \ldots, 0.999)$

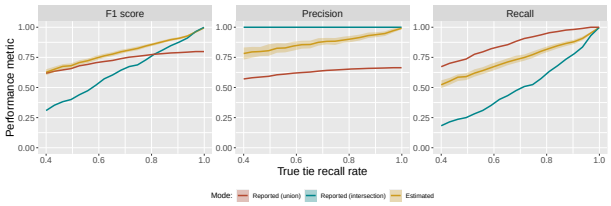

(d) Standard deviation of recall of true tie rate, $\in (0.001, \ldots, 2)$

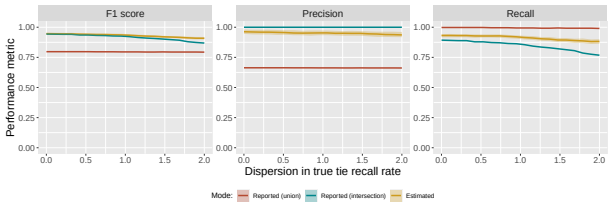

(e) Average false positive rate, $\in (0.001, \ldots, 0.02)$, and average recall of true tie rate, $\in (0.999, \ldots, 0.4)$

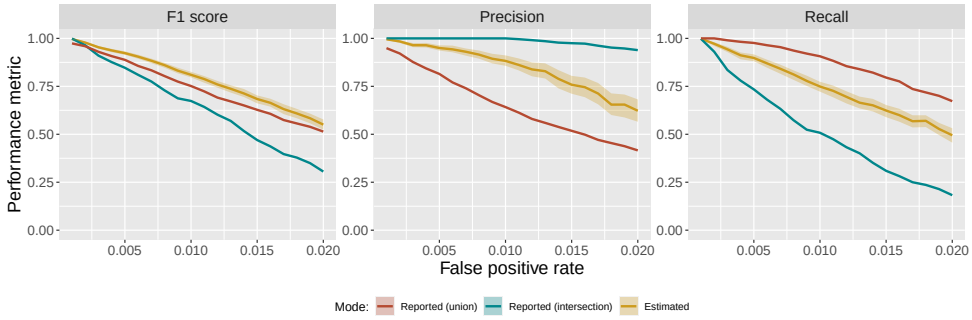

Fig. 12: Edge-wise classification accuracy in the base model, according to precision (the sum of true positive classifications divided by the sum of true and false positives), recall (the sum of true positive classifications divided by the sum of true positives and false negatives), and F1 (the harmonic mean of precision and recall rates) metrics.

(a) Average false positive rate, $\in (0.001, \ldots, 0.05)$

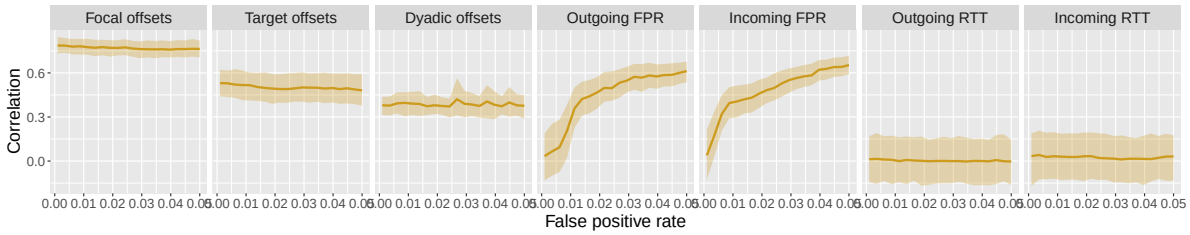

(b) Standard deviation of false positive rate, $\in (0.001, \ldots, 2)$

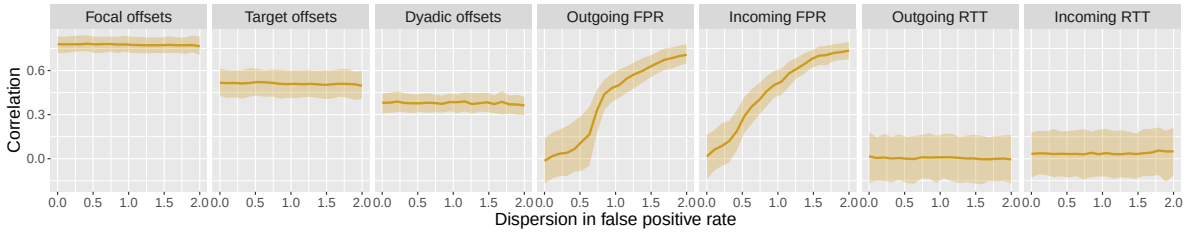

(c) Average recall of true tie rate, $\in (0.4, \ldots, 0.999)$

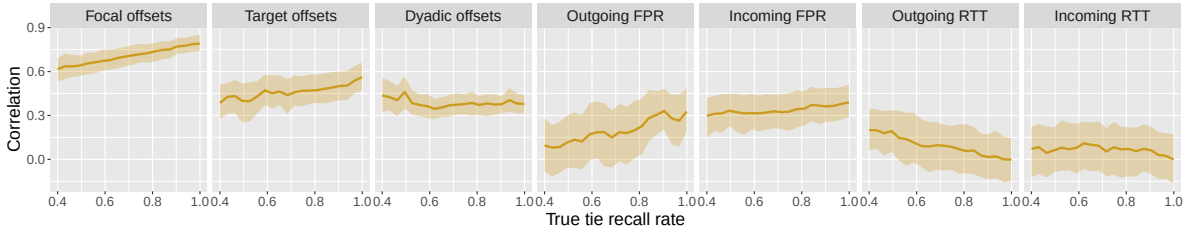

(d) Standard deviation of recall of true tie rate, $\in (0.001, \ldots, 2)$

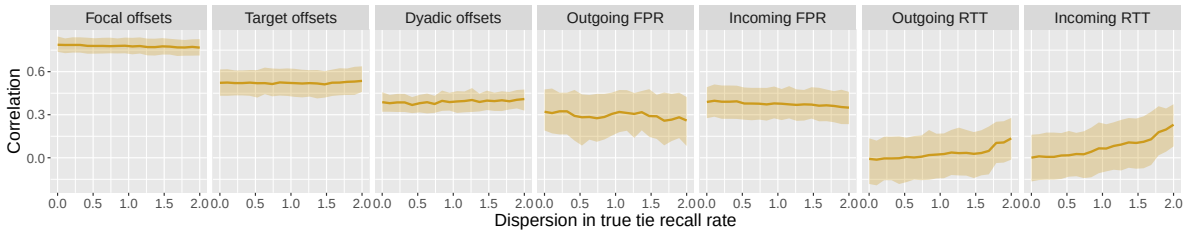

(e) Average false positive rate, $\in (0.001, \ldots, 0.02)$, and average recall of true tie rate, $\in (0.999, \ldots, 0.4)$

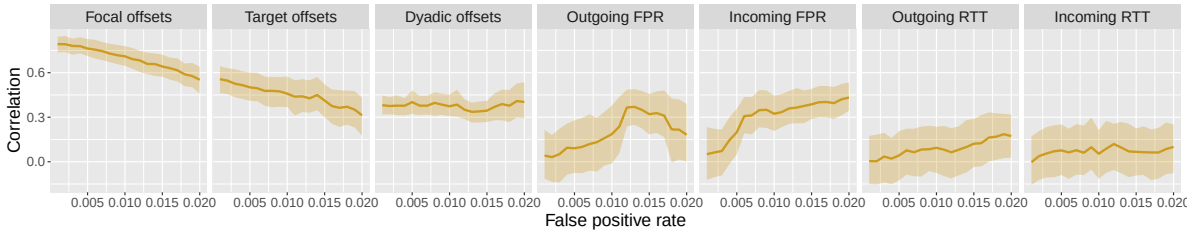

Fig. 13: Individual-level parameter recovery from the base model. Each frame plots the correlation between generative parameter values and those estimated by our latent network model. The y-axis of each sub-figure represents the correlation between the generative and estimated parameter values, and the x-axis represents the value of the focal simulation parameter given in the subheading. For example, the x-axis in figure 13a represents the average false positive rate used when simulating the reported network data.

(a) Average false positive rate, $\in (0.001, \ldots, 0.05)$

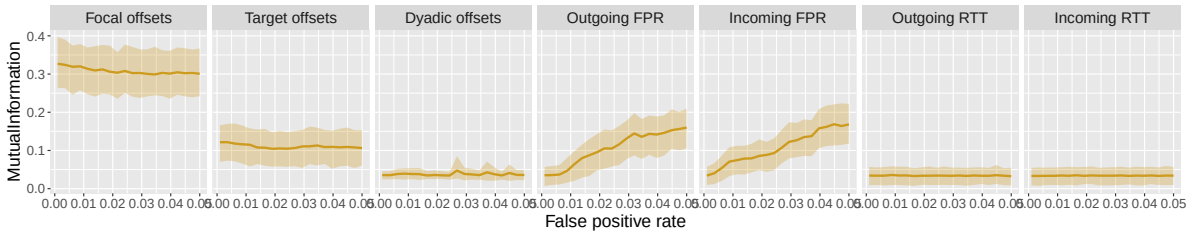

(b) Standard deviation of false positive rate, $\in (0.001, \ldots, 2)$

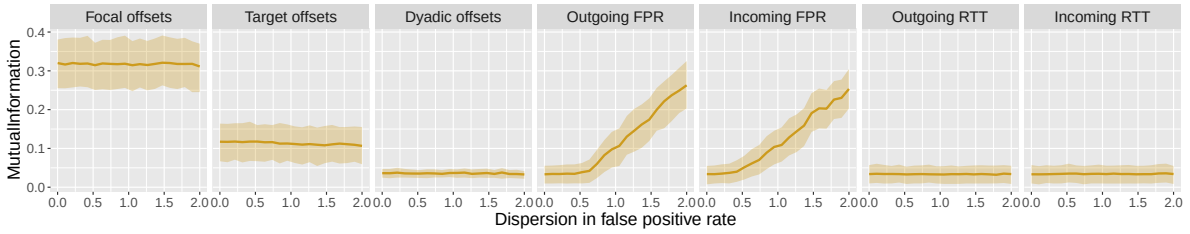

(c) Average recall of true tie rate, $\in (0.4, \ldots, 0.999)$

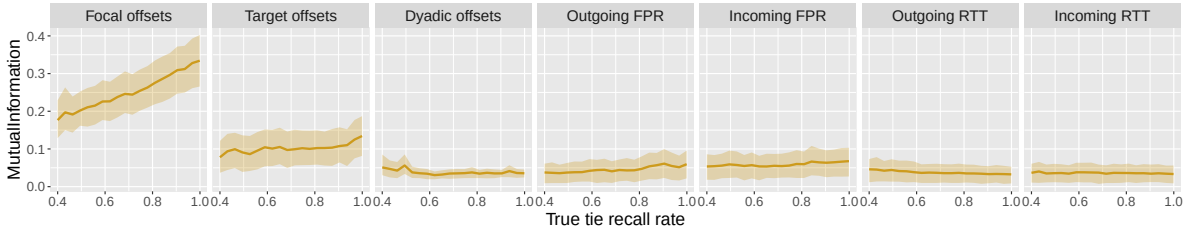

(d) Standard deviation of recall of true tie rate, $\in (0.001, \ldots, 2)$

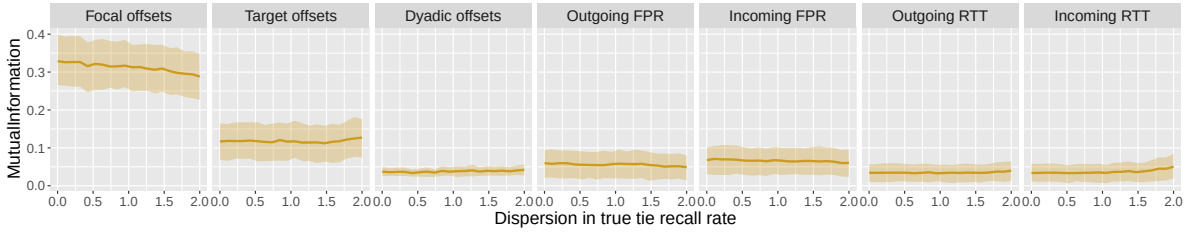

(e) Average false positive rate, $\in (0.001, \ldots, 0.02)$, and average recall of true tie rate, $\in (0.999, \ldots, 0.4)$

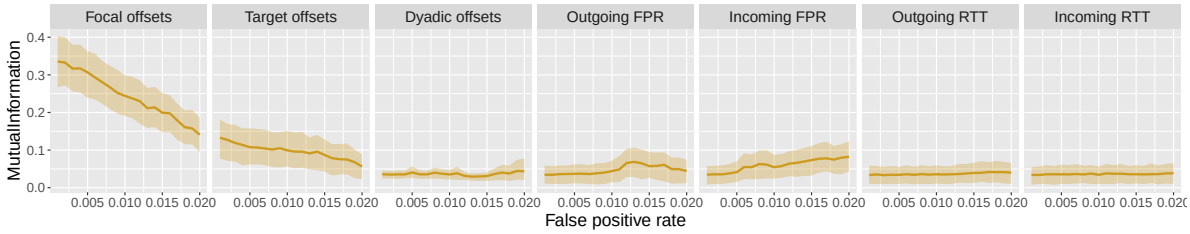

Fig. 14: Individual-level parameter recovery from the base model. Each frame plots the mutual information between generative parameter values and those estimated by our latent network model. The y-axis of each sub-figure represents the mutual information between the generative and estimated parameter values, and the x-axis represents the value of the focal simulation parameter given in the subheading. For example, the x-axis in figure 14a represents the average false positive rate used when simulating the reported network data.

(a) Average false positive rate, $\in (0.001, \ldots, 0.05)$

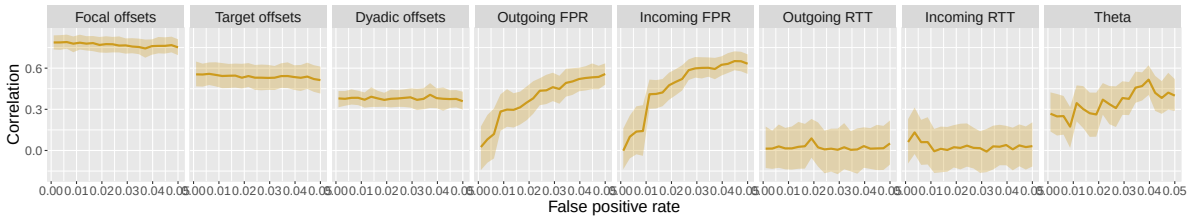

(b) Standard deviation of false positive rate, $\in (0.001, \ldots, 2)$

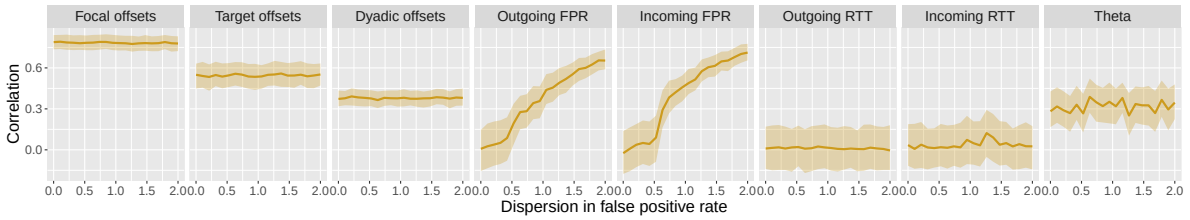

(c) Average recall of true tie rate, $\in (0.4, \ldots, 0.999)$

(d) Standard deviation of recall of true tie rate, $\in (0.001, \ldots, 2)$

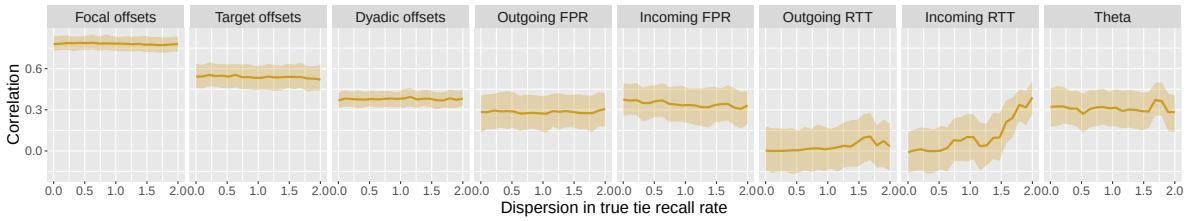

(e) Average false positive rate, $\in (0.001, \ldots, 0.02)$, and average recall of true tie rate, $\in (0.999, \ldots, 0.4)$

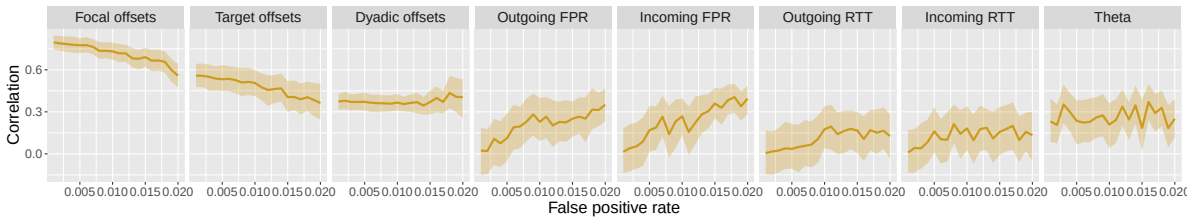

Fig. 15: Individual-level parameter recovery from the model that includes question order bias. Each frame plots the correlation between generative parameter values and those estimated by our latent network model. The y-axis of each sub-figure represents the correlation between the generative and estimated parameter values, and the x-axis represents the value of the focal simulation parameter given in the subheading. For example, the x-axis in figure 16a represents the average false positive rate used when simulating the reported network data.

(a) Average false positive rate, $\in (0.001, \ldots, 0.05)$

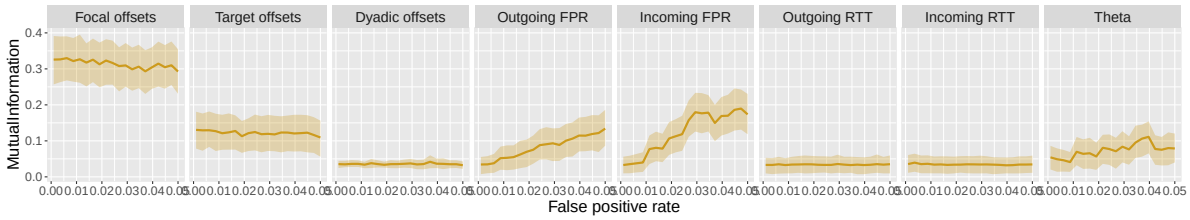

(b) Standard deviation of false positive rate, $\in (0.001, \ldots, 2)$

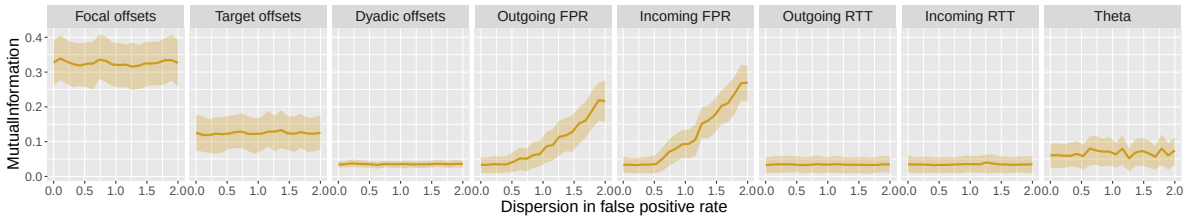

(c) Average recall of true tie rate, $\in (0.4, \ldots, 0.999)$

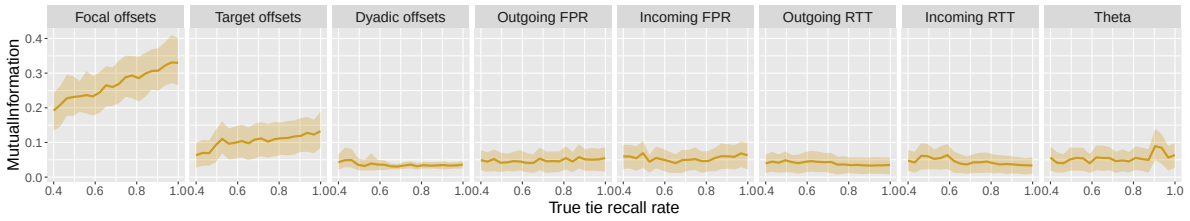

(d) Standard deviation of recall of true tie rate, $\in (0.001, \ldots, 2)$

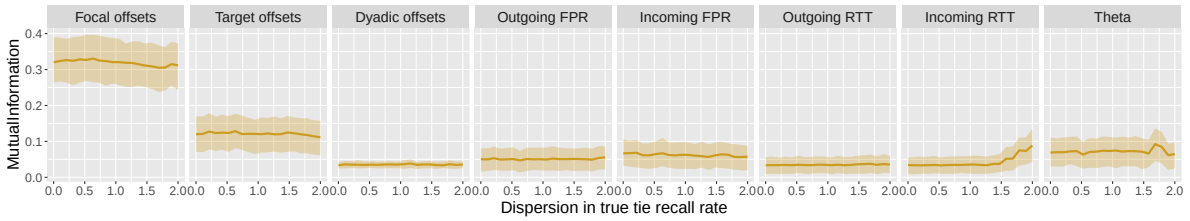

(e) Average false positive rate, $\in (0.001, \ldots, 0.02)$, and average recall of true tie rate, $\in (0.999, \ldots, 0.4)$

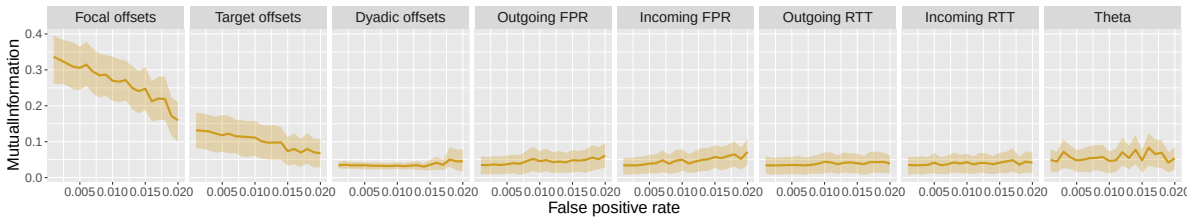

Fig. 16: Individual-level parameter recovery from the model that includes question order bias. Each frame plots the mutual information between generative parameter values and those estimated by our latent network model. The y-axis of each sub-figure represents the mutual information between the generative and estimated parameter values, and the x-axis represents the value of the focal simulation parameter given in the subheading. For example, the x-axis in figure 15a represents the average false positive rate used when simulating the reported network data.

(a) Average false positive rate, $\in (0.001, \ldots, 0.05)$

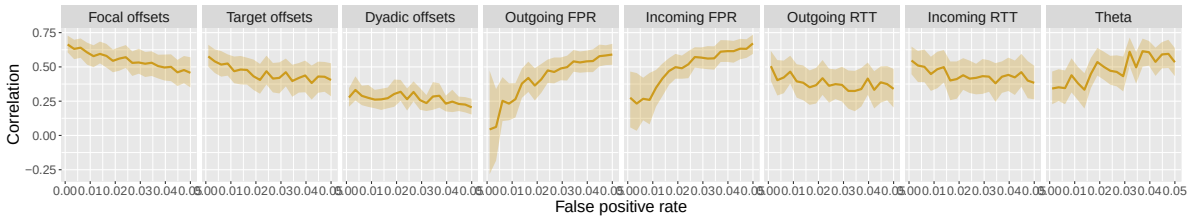

(b) Standard deviation of false positive rate, $\in (0.001, \ldots, 2)$

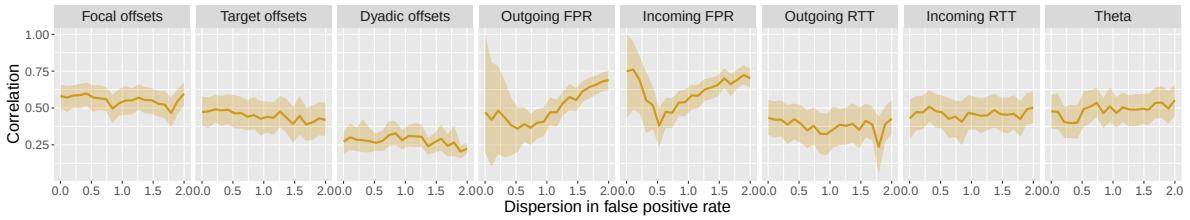

(c) Average recall of true tie rate, $\in (0.4, \ldots, 0.999)$

(d) Standard deviation of recall of true tie rate, $\in (0.001, \ldots, 2)$

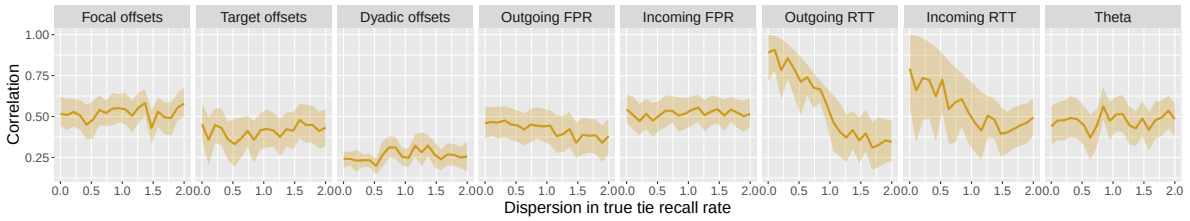

(e) Average false positive rate, $\in (0.001, \ldots, 0.02)$, and average recall of true tie rate, $\in (0.999, \ldots, 0.4)$

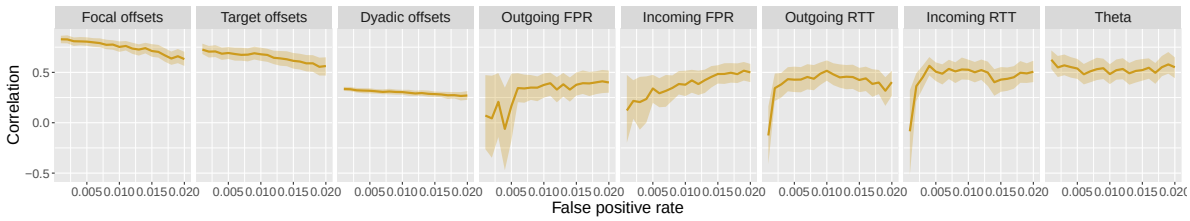

Fig. 17: Individual-level parameter recovery from the model that includes an attribute-related bias. Each frame plots the correlation between generative parameter values and those estimated by our latent network model. The y-axis of each sub-figure represents the correlation between the generative and estimated parameter values, and the x-axis represents the value of the focal simulation parameter given in the subheading. For example, the x-axis in figure 17a represents the average false positive rate used when simulating the reported network data.

(a) Average false positive rate, $\in (0.001, \ldots, 0.05)$

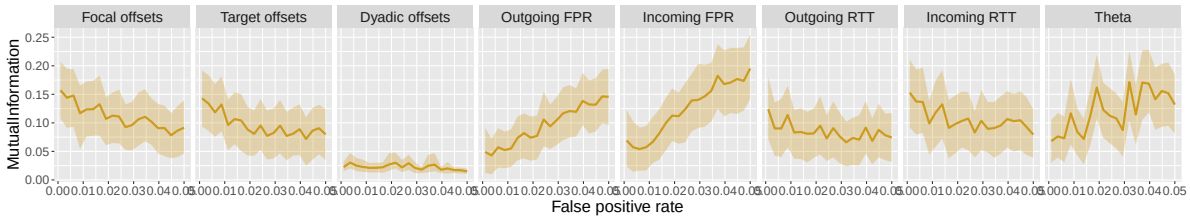

(b) Standard deviation of false positive rate, $\in (0.001, \ldots, 2)$

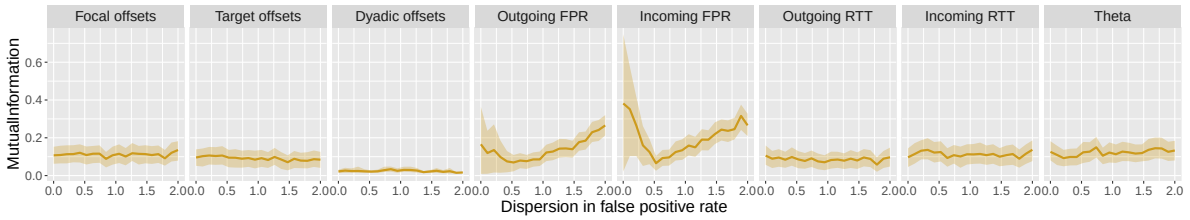

(c) Average recall of true tie rate, $\in (0.4, \ldots, 0.999)$

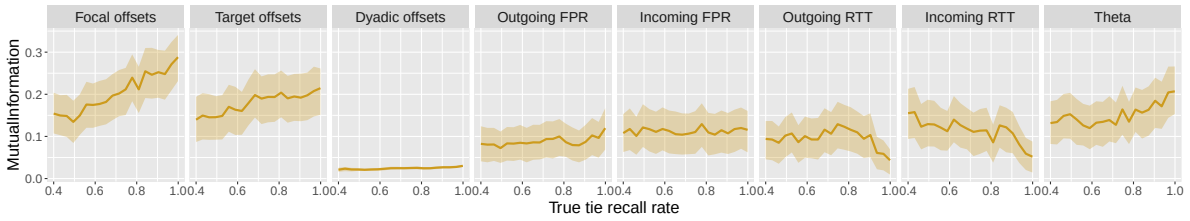

(d) Standard deviation of recall of true tie rate, $\in (0.001, \ldots, 2)$

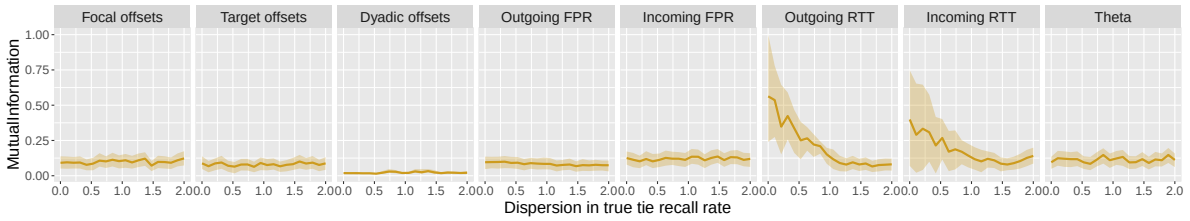

(e) Average false positive rate, $\in (0.001, \ldots, 0.02)$, and average recall of true tie rate, $\in (0.999, \ldots, 0.4)$

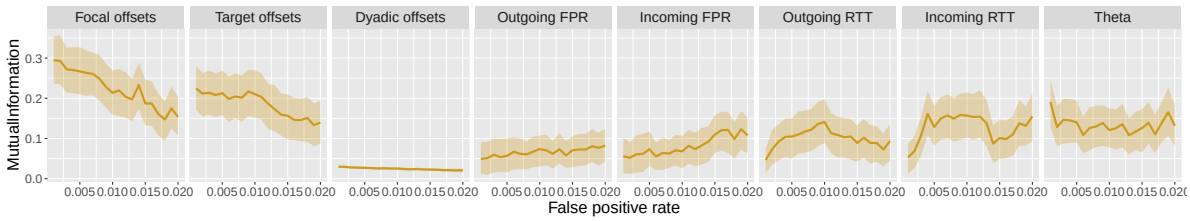

Fig. 18: Individual-level parameter recovery from the model that includes an attribute-related bias. Each frame plots the mutual information between generative parameter values and those estimated by our latent network model. The y-axis of each sub-figure represents the mutual information between the generative and estimated parameter values, and the x-axis represents the value of the focal simulation parameter given in the subheading. For example, the x-axis in figure 18a represents the average false positive rate used when simulating the reported network data.

(a) Average false positive rate, $\in (0.001, \ldots, 0.05)$

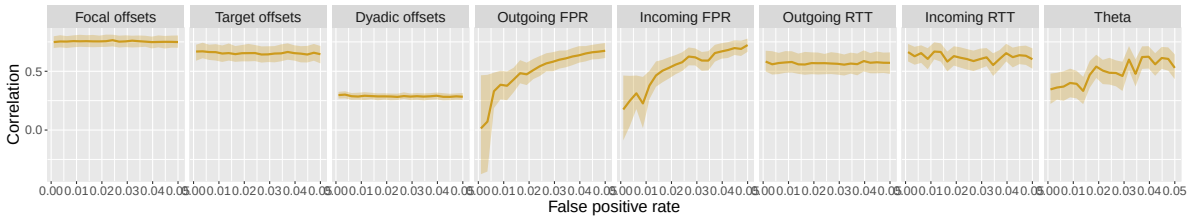

(b) Standard deviation of false positive rate, $\in (0.001, \ldots, 2)$

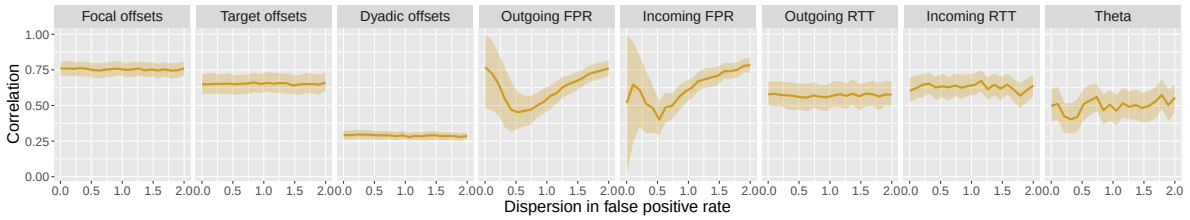

(c) Average recall of true tie rate, $\in (0.4, \ldots, 0.999)$

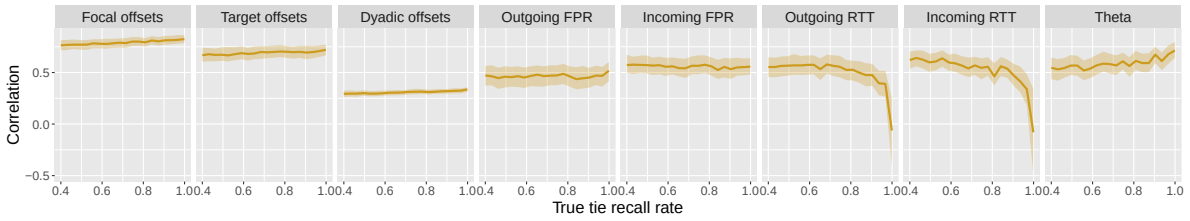

(d) Standard deviation of recall of true tie rate, $\in (0.001, \ldots, 2)$

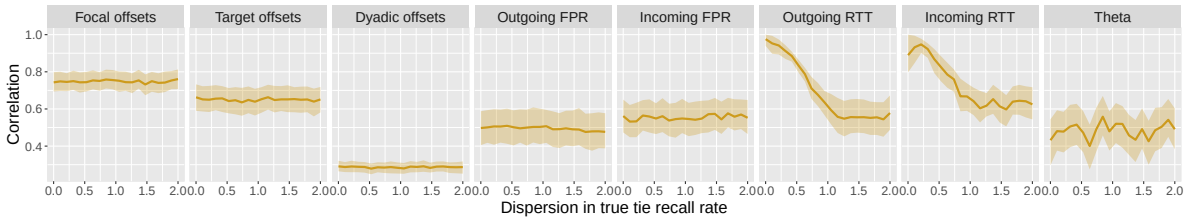

(e) Average false positive rate, $\in (0.001, \ldots, 0.02)$, and average recall of true tie rate, $\in (0.999, \ldots, 0.4)$

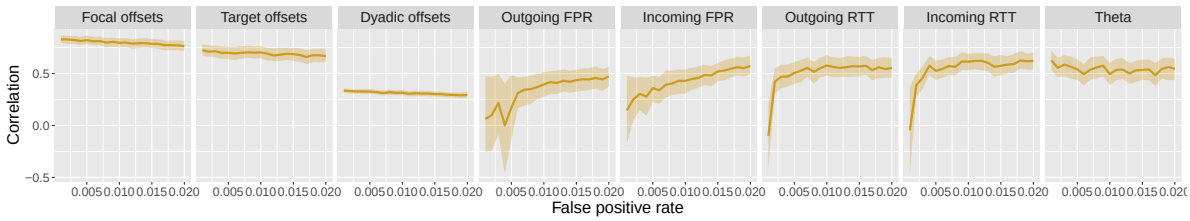

Fig. 19: Individual-level parameter recovery from the model that includes a 'ground truth' network layer. Each frame plots the correlation between generative parameter values and those estimated by our latent network model. The y-axis of each sub-figure represents the correlation between the generative and estimated parameter values, and the x-axis represents the value of the focal simulation parameter given in the subheading. For example, the x-axis in figure 19a represents the average false positive rate used when simulating the reported network data.

(a) Average false positive rate, $\in (0.001, \ldots, 0.05)$

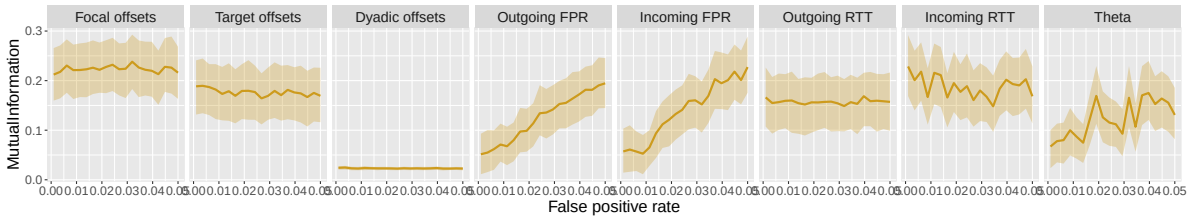

(b) Standard deviation of false positive rate, $\in (0.001, \ldots, 2)$

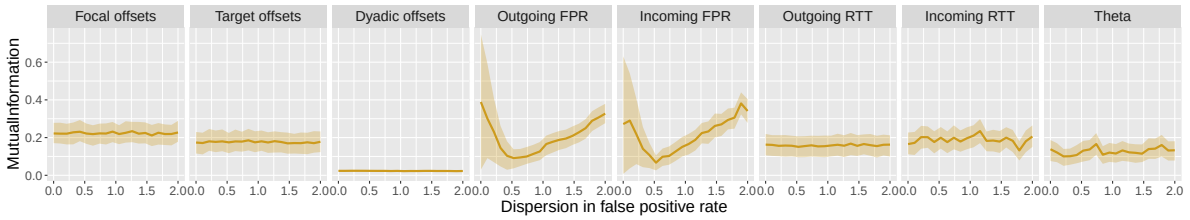

(c) Average recall of true tie rate, $\in (0.4, \ldots, 0.999)$

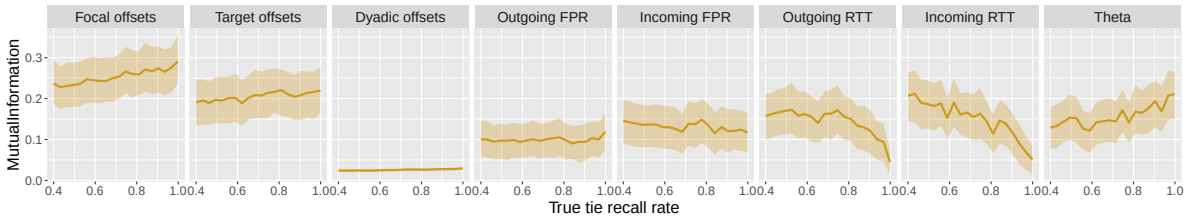

(d) Standard deviation of recall of true tie rate, $\in (0.001, \ldots, 2)$

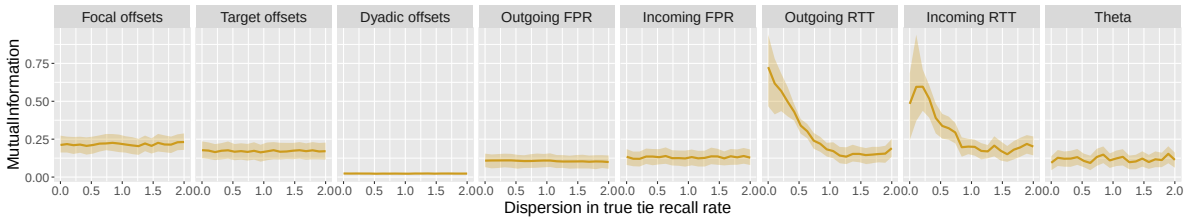

(e) Average false positive rate, $\in (0.001, \ldots, 0.02)$, and average recall of true tie rate, $\in (0.999, \ldots, 0.4)$

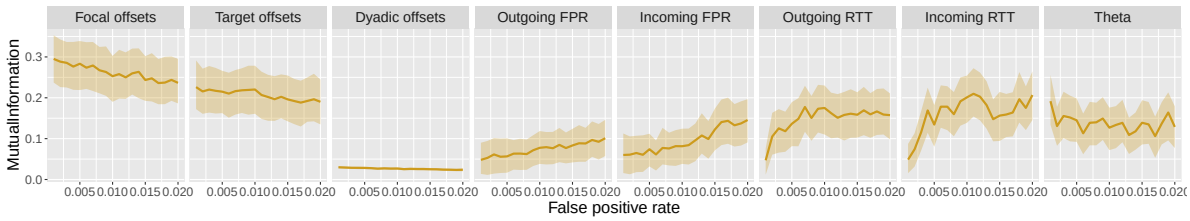

Fig. 20: Individual-level parameter recovery from the model that includes a 'ground truth' network layer. Each frame plots the mutual information between generative parameter values and those estimated by our latent network model. The y-axis of each sub-figure represents the mutual information between the generative and estimated parameter values, and the x-axis represents the value of the focal simulation parameter given in the subheading. For example, the x-axis in figure 20a represents the average false positive rate used when simulating the reported network data.

(a) Average false positive rate, $\in (0.001, \ldots, 0.05)$

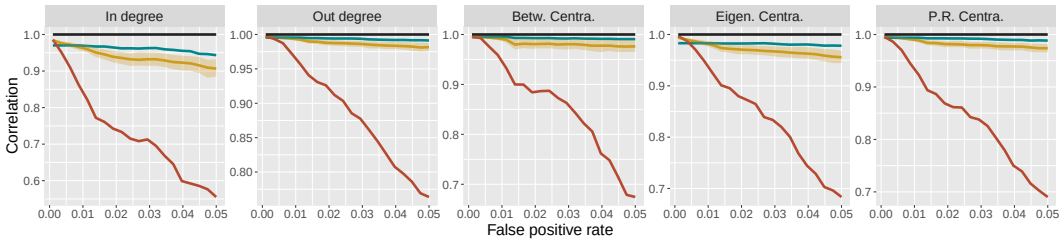

(b) Standard deviation of false positive rate, $\in (0.001, \ldots, 2)$

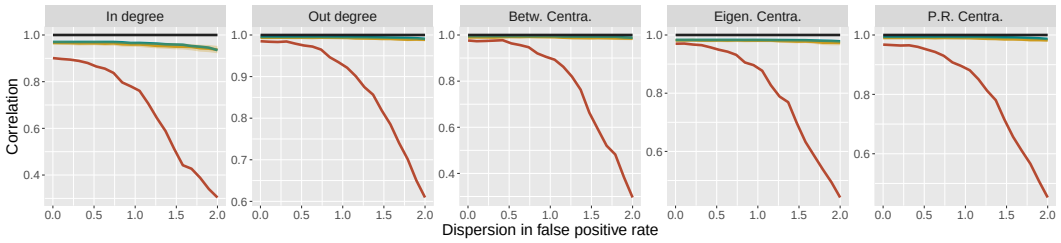

(c) Average recall of true tie rate, $\in (0.4, \ldots, 0.999)$

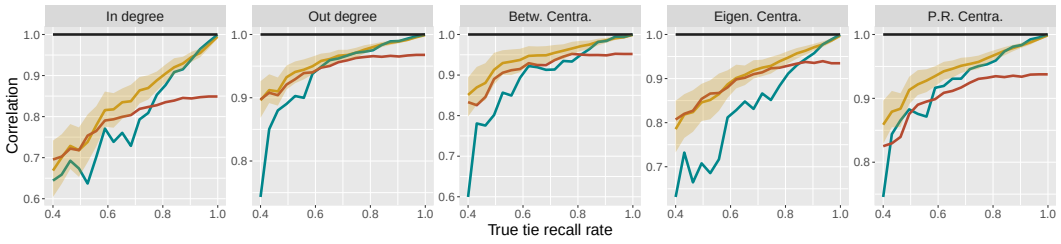

(d) Standard deviation of recall of true tie rate, $\in (0.001, \ldots, 2)$

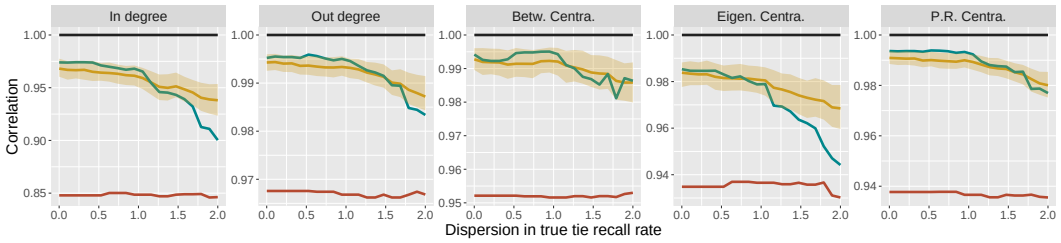

(e) Average false positive rate, $\in (0.001, \ldots, 0.02)$, and average recall of true tie rate, $\in (0.999, \ldots, 0.4)$

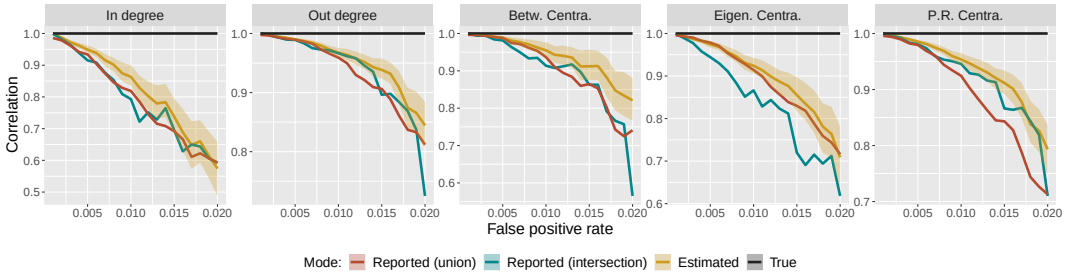

Fig. 21: Correlation between node-level properties of the 'true' network and node-level properties as calculated via three different network reconstruction methods (base model). The yellow curves show the correlation between the node-level properties inferred using our latent network model, the red curves show the same measures inferred using the union of reported data, and the blue curves show the same measures inferred using the intersection of reported data. The y-axis of each sub-figure represents the correlation between the 'true' node-level metrics and the node-level metrics estimated with each reconstruction method, and the x-axis represents the value of the focal simulation parameter given in the subheading. For example, the x-axis in figure 21a represents the average false positive rate used when simulating the reported network data.

(a) Average false positive rate, $\in (0.001, \ldots, 0.05)$

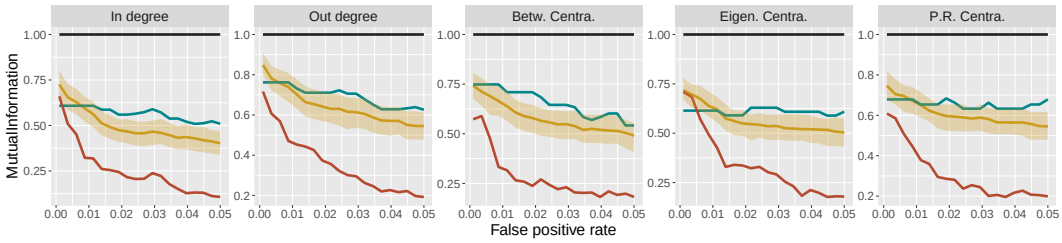

(b) Standard deviation of false positive rate, $\in (0.001, \ldots, 2)$

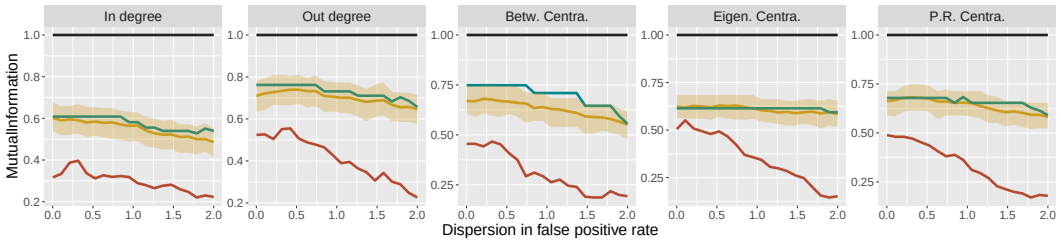

(c) Average recall of true tie rate, $\in (0.4, \ldots, 0.999)$

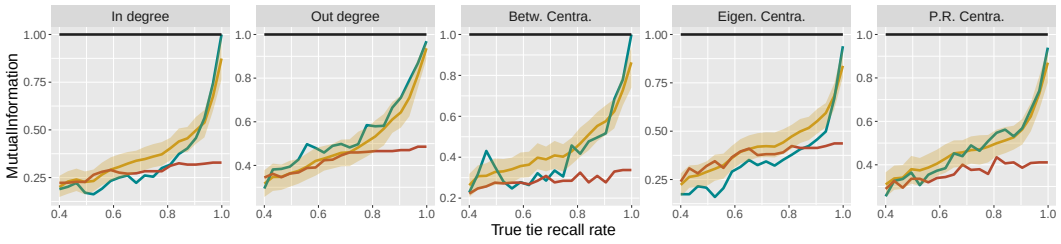

(d) Standard deviation of recall of true tie rate, $\in (0.001, \ldots, 2)$

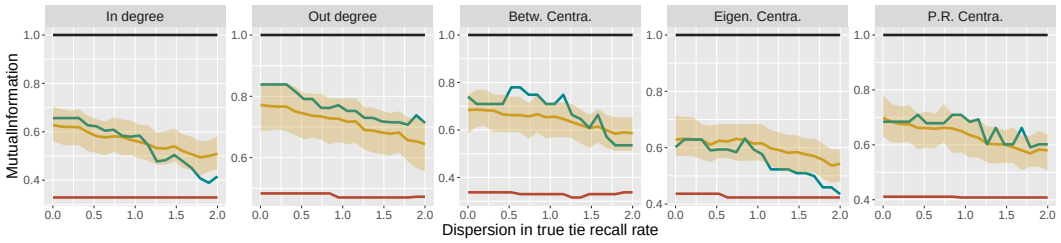

(e) Average false positive rate, $\in (0.001, \ldots, 0.02)$, and average recall of true tie rate, $\in (0.999, \ldots, 0.4)$

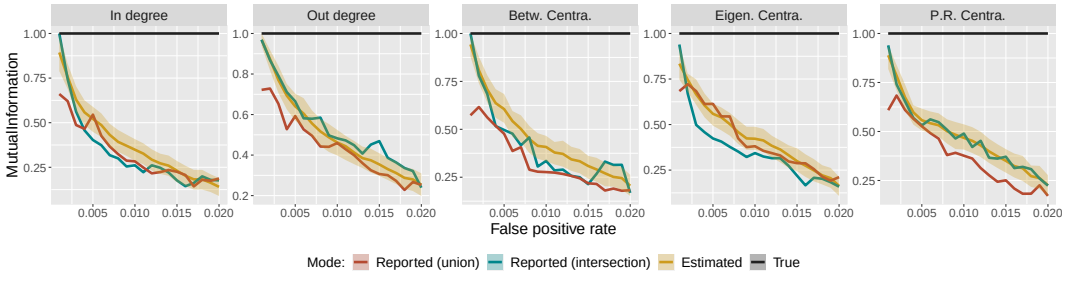

Fig. 22: Mutual information between node-level properties of the 'true' network and node-level properties as calculated via three different network reconstruction methods (base model). The yellow curves show the mutual information between the node-level properties inferred using our latent network model, the red curves show the same measures inferred using the union of reported data, and the blue curves show the same measures inferred using the intersection of reported data. The y-axis of each sub-figure represents the correlation between the 'true' node-level metrics and the node-level metrics estimated with each reconstruction method, and the x-axis represents the value of the focal simulation parameter given in the subheading. For example, the x-axis in figure 22a represents the average false positive rate used when simulating the reported network data.

(a) Average false positive rate, $\in (0.001, \ldots, 0.05)$

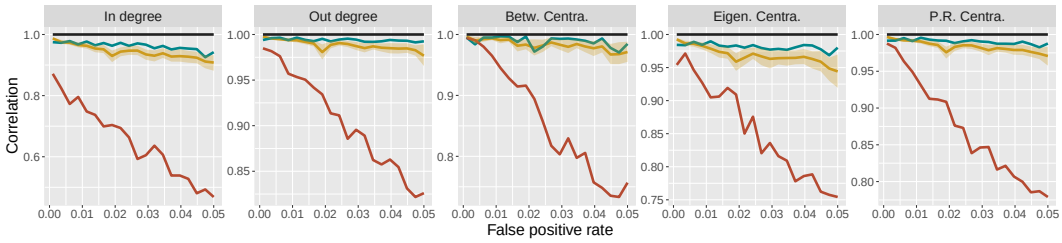

(b) Standard deviation of false positive rate, $\in (0.001, \ldots, 2)$

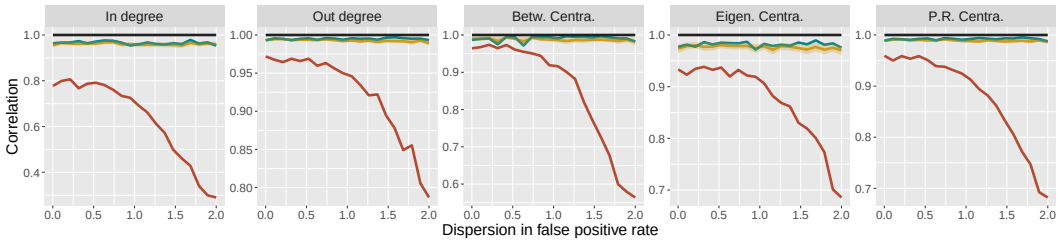

(c) Average recall of true tie rate, $\in (0.4, \ldots, 0.999)$

(d) Standard deviation of recall of true tie rate, $\in (0.001, \ldots, 2)$

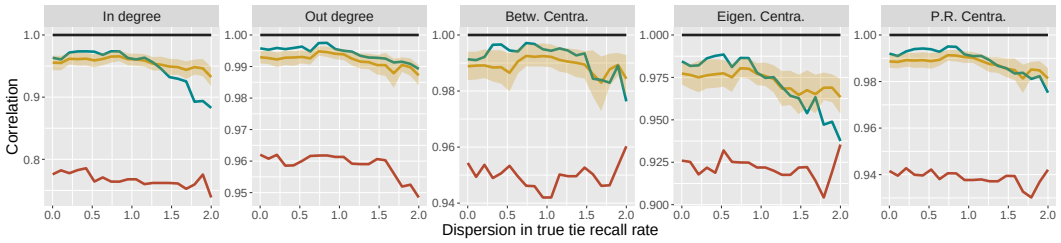

(e) Average false positive rate, $\in (0.001, \ldots, 0.02)$, and average recall of true tie rate, $\in (0.999, \ldots, 0.4)$

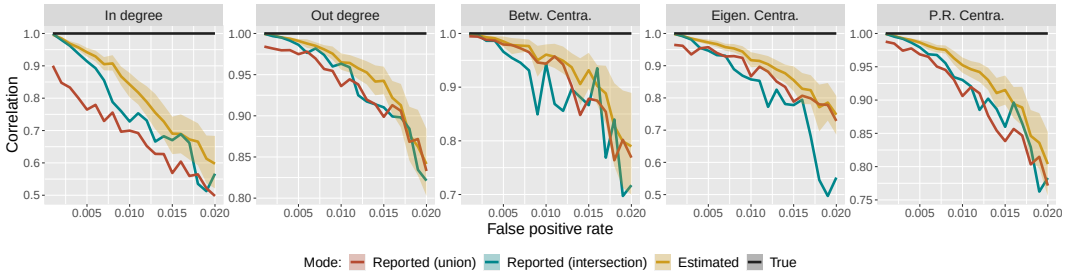

Fig. 23: Correlation between node-level properties of the 'true' network and node-level properties as calculated via three different network reconstruction methods (model with question order bias). The yellow curves show the correlation between the node-level properties inferred using our latent network model, the red curves show the same measures inferred using the union of reported data, and the blue curves show the same measures inferred using the intersection of reported data. The y-axis of each sub-figure represents the correlation between the 'true' node-level metrics and the node-level metrics estimated with each reconstruction method, and the x-axis represents the value of the focal simulation parameter given in the subheading. For example, the x-axis in figure 23a represents the average false positive rate used when simulating the reported network data.

(a) Average false positive rate, $\in (0.001, \ldots, 0.05)$

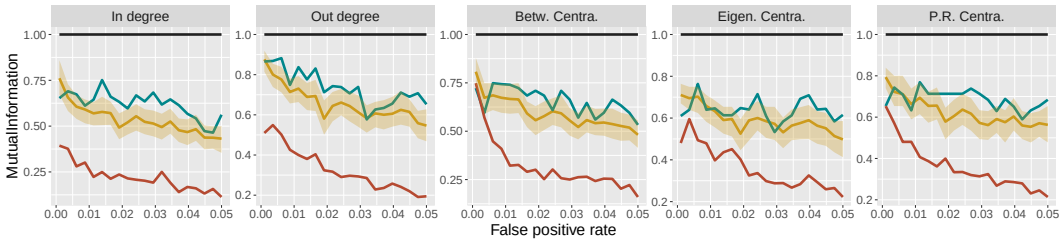

(b) Standard deviation of false positive rate, $\in (0.001, \ldots, 2)$

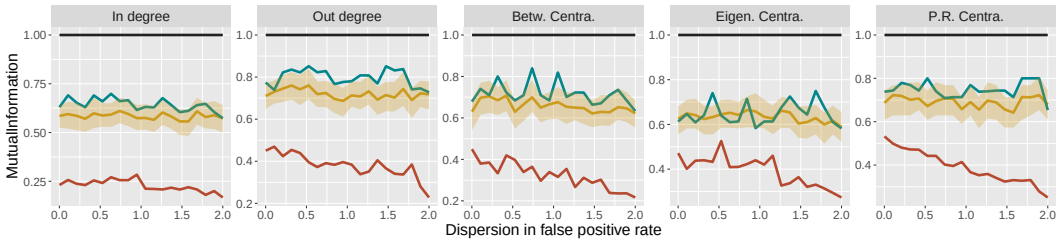

(c) Average recall of true tie rate, $\in (0.4, \ldots, 0.999)$

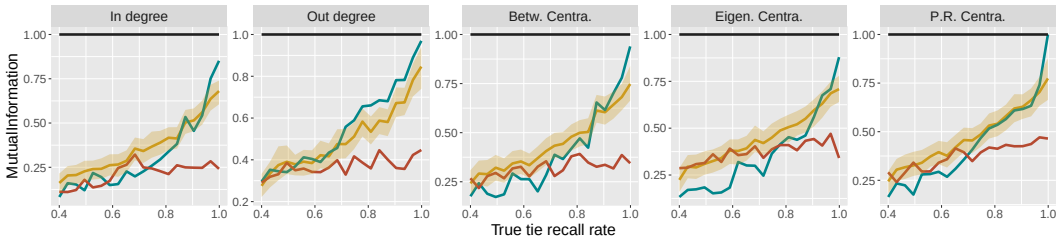

(d) Standard deviation of recall of true tie rate, $\in (0.001, \ldots, 2)$

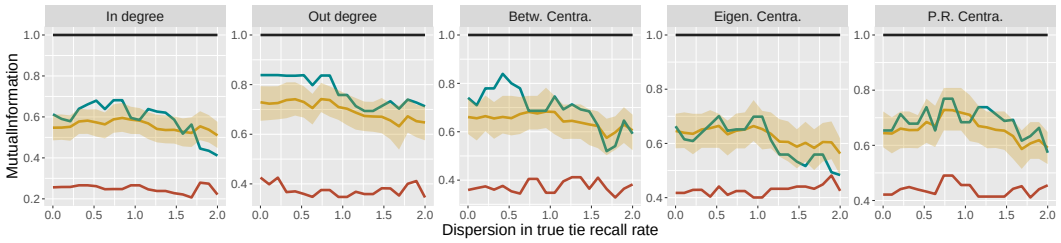

(e) Average false positive rate, $\in (0.001, \ldots, 0.02)$, and average recall of true tie rate, $\in (0.999, \ldots, 0.4)$

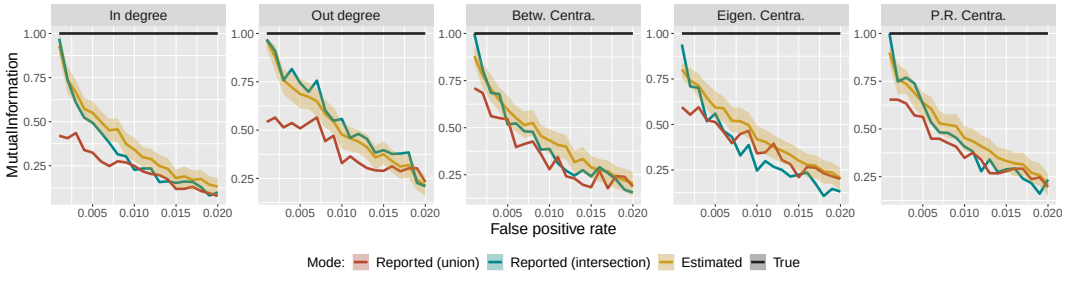

Fig. 24: Mutual information between node-level properties of the 'true' network and node-level properties as calculated via three different network reconstruction methods (model with question order bias). The yellow curves show the mutual information between the node-level properties inferred using our latent network model, the red curves show the same measures inferred using the union of reported data, and the blue curves show the same measures inferred using the intersection of reported data. The y-axis of each sub-figure represents the correlation between the 'true' node-level metrics and the node-level metrics estimated with each reconstruction method, and the x-axis represents the value of the focal simulation parameter given in the subheading. For example, the x-axis in figure 24a represents the average false positive rate used when simulating the reported network data.

(a) Average false positive rate, $\in (0.001, \ldots, 0.05)$

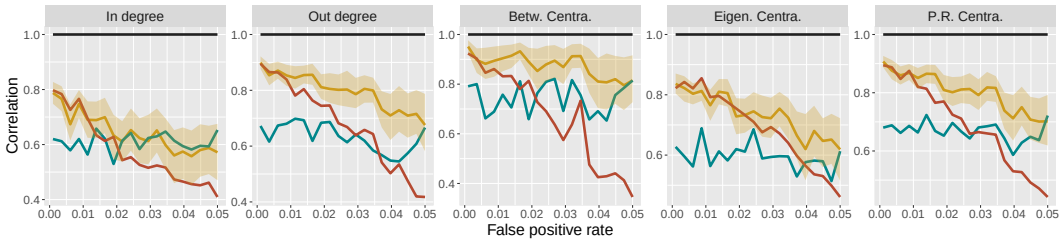

(b) Standard deviation of false positive rate, $\in (0.001, \ldots, 2)$

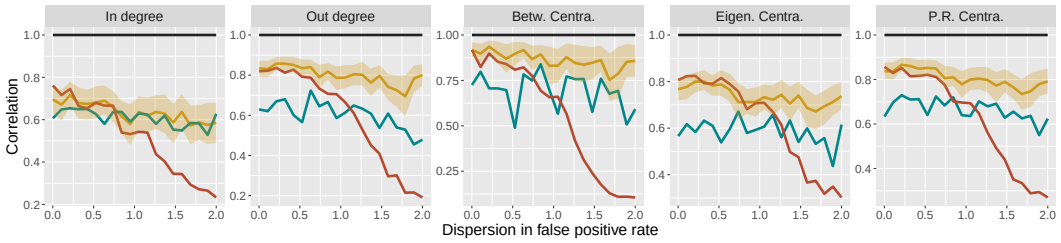

(c) Average recall of true tie rate, $\in (0.4, \ldots, 0.999)$

(d) Standard deviation of recall of true tie rate, $\in (0.001, \ldots, 2)$

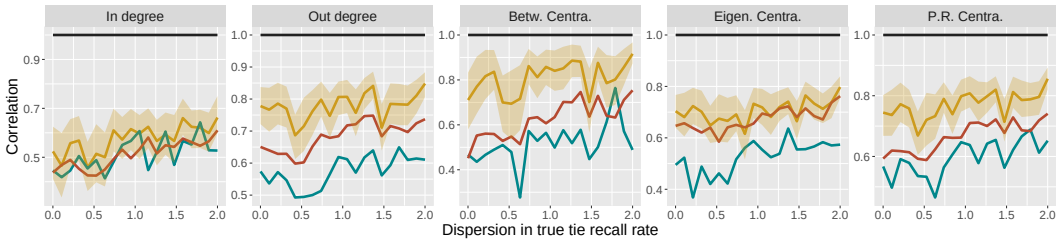

(e) Average false positive rate, $\in (0.001, \ldots, 0.02)$, and average recall of true tie rate, $\in (0.999, \ldots, 0.4)$

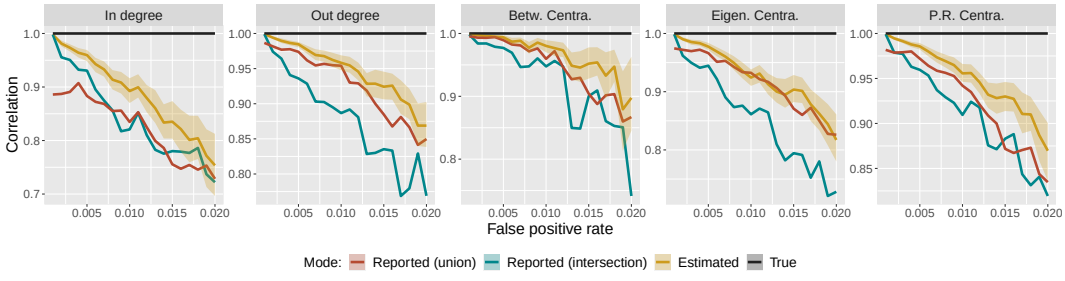

Fig. 25: Correlation between node-level properties of the 'true' network and node-level properties as calculated via three different network reconstruction methods (model with attribute-related bias). The yellow curves show the correlation between the node-level properties inferred using our latent network model, the red curves show the same measures inferred using the union of reported data, and the blue curves show the same measures inferred using the intersection of reported data. The y-axis of each sub-figure represents the correlation between the 'true' node-level metrics and the node-level metrics estimated with each reconstruction method, and the x-axis represents the value of the focal simulation parameter given in the subheading. For example, the x-axis in figure 25a represents the average false positive rate used when simulating the reported network data.

(a) Average false positive rate, $\in (0.001, \ldots, 0.05)$

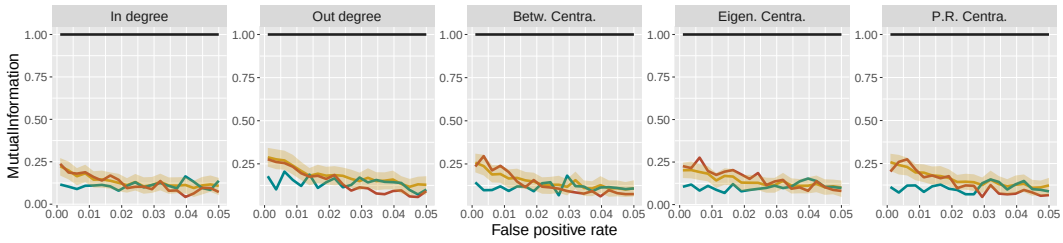

(b) Standard deviation of false positive rate, $\in (0.001, \ldots, 2)$

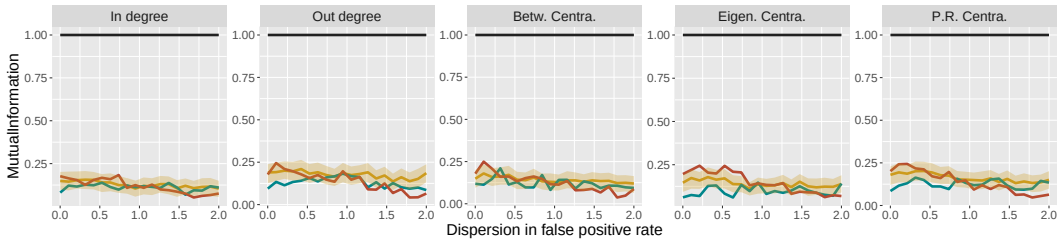

(c) Average recall of true tie rate, $\in (0.4, \ldots, 0.999)$

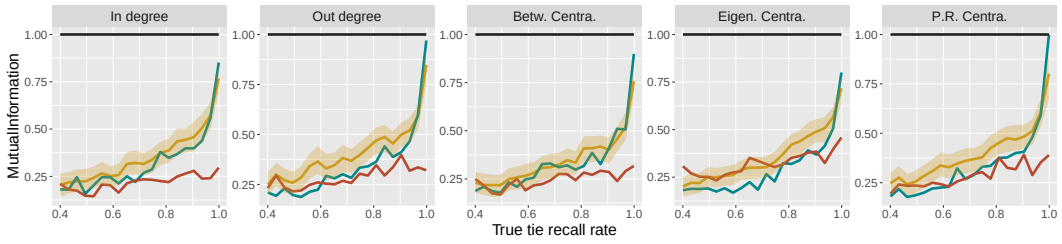

(d) Standard deviation of recall of true tie rate, $\in (0.001, \ldots, 2)$

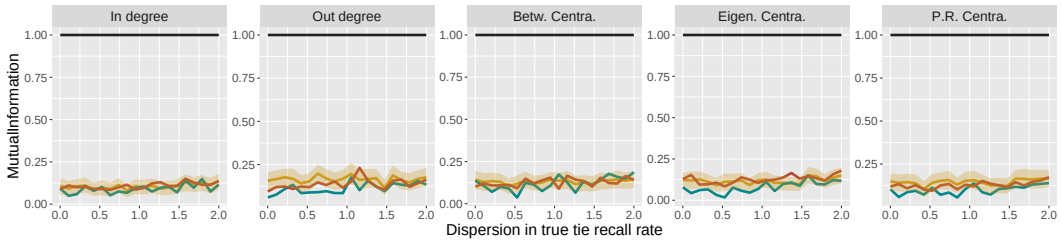

(e) Average false positive rate, $\in (0.001, \ldots, 0.02)$, and average recall of true tie rate, $\in (0.999, \ldots, 0.4)$

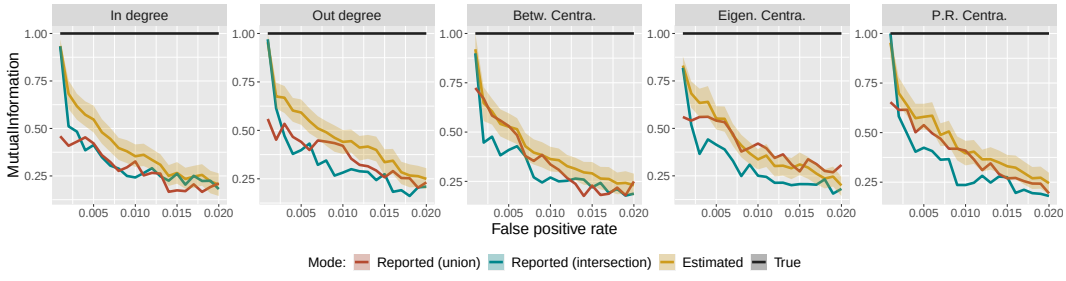

Fig. 26: Mutual information between node-level properties of the 'true' network and node-level properties as calculated via three different network reconstruction methods (model with attribute-related bias). The yellow curves show the mutual information between the node-level properties inferred using our latent network model, the red curves show the same measures inferred using the union of reported data, and the blue curves show the same measures inferred using the intersection of reported data. The y-axis of each sub-figure represents the correlation between the 'true' node-level metrics and the node-level metrics estimated with each reconstruction method, and the x-axis represents the value of the focal simulation parameter given in the subheading. For example, the x-axis in figure 26a represents the average false positive rate used when simulating the reported network data.

(a) Average false positive rate, $\in (0.001, \ldots, 0.05)$

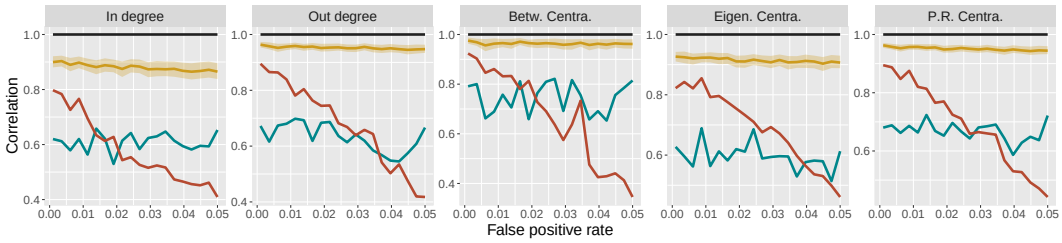

(b) Standard deviation of false positive rate, $\in (0.001, \ldots, 2)$

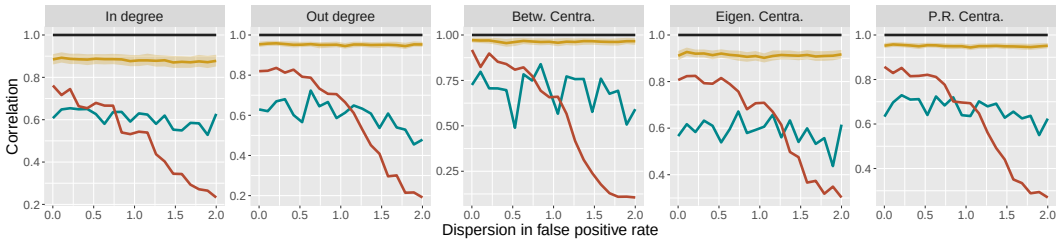

(c) Average recall of true tie rate, $\in (0.4, \ldots, 0.999)$

(d) Standard deviation of recall of true tie rate, $\in (0.001, \ldots, 2)$

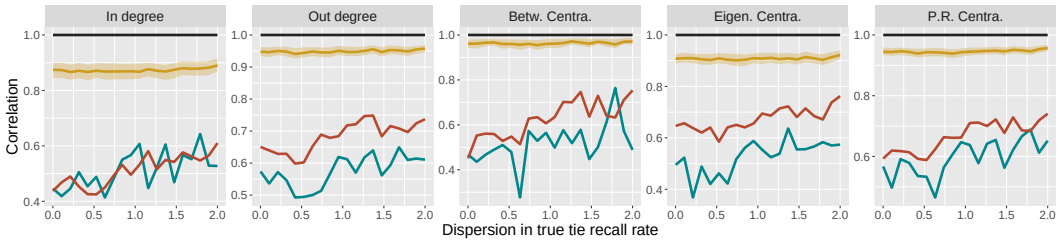

(e) Average false positive rate, $\in (0.001, \ldots, 0.02)$, and average recall of true tie rate, $\in (0.999, \ldots, 0.4)$

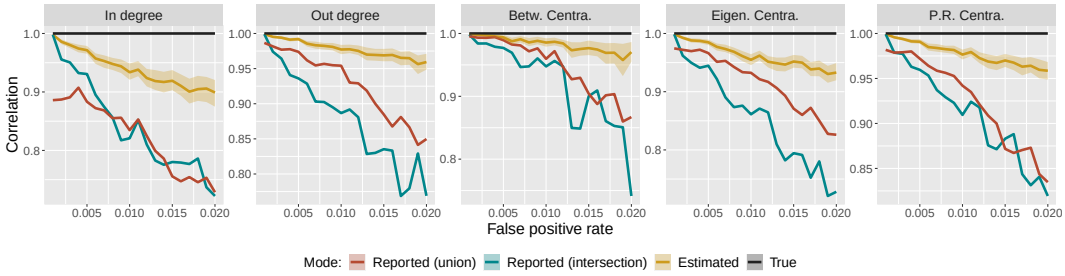

Fig. 27: Correlation between node-level properties of the 'true' network and node-level properties as calculated via three different network reconstruction methods (model which integrates 'ground truth' data). The yellow curves show the correlation between the node-level properties inferred using our latent network model, the red curves show the same measures inferred using the union of reported data, and the blue curves show the same measures inferred using the intersection of reported data. The y-axis of each sub-figure represents the correlation between the 'true' node-level metrics and the node-level metrics estimated with each reconstruction method, and the x-axis represents the value of the focal simulation parameter given in the subheading. For example, the x-axis in figure 27a represents the average false positive rate used when simulating the reported network data.

(a) Average false positive rate, $\in (0.001, \ldots, 0.05)$

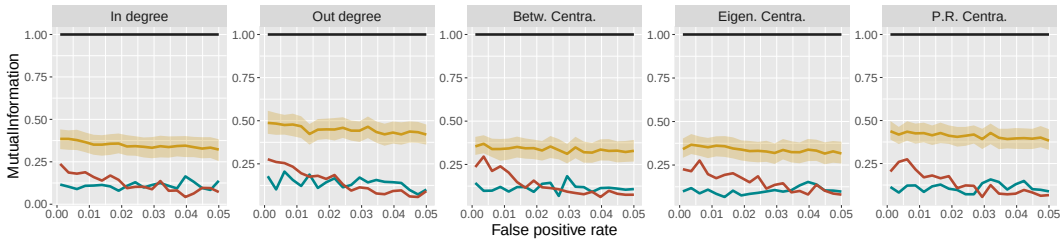

(b) Standard deviation of false positive rate, $\in (0.001, \ldots, 2)$

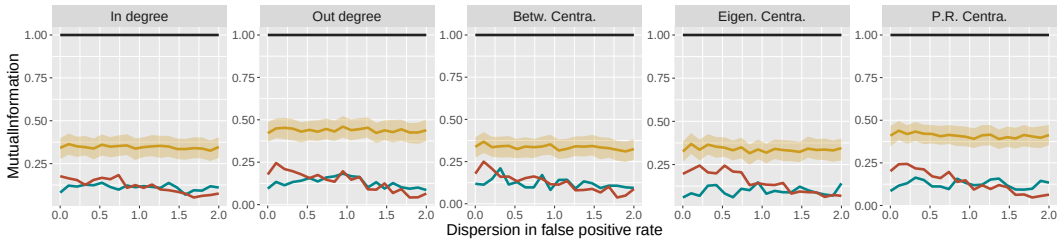

(c) Average recall of true tie rate, $\in (0.4, \ldots, 0.999)$

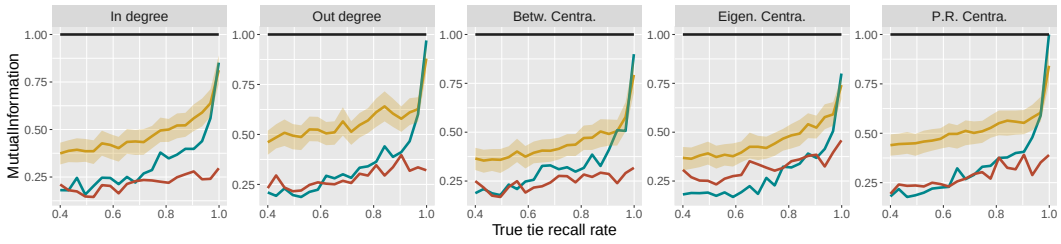

(d) Standard deviation of recall of true tie rate, $\in (0.001, \ldots, 2)$

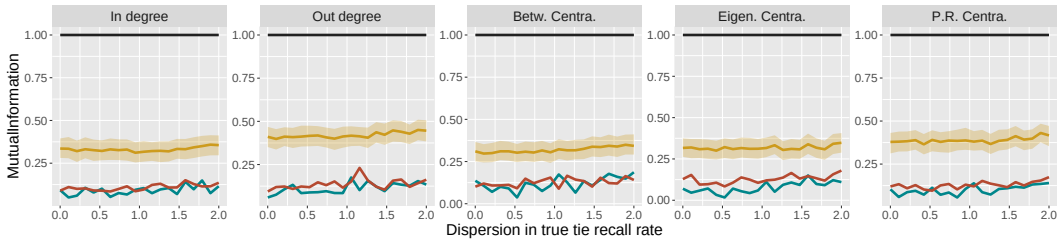

(e) Average false positive rate, $\in (0.001, \ldots, 0.02)$, and average recall of true tie rate, $\in (0.999, \ldots, 0.4)$

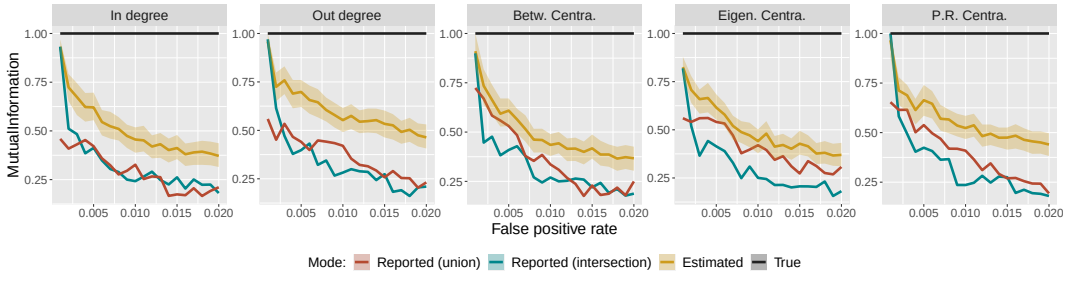

Fig. 28: Mutual information between node-level properties of the 'true' network and node-level properties as calculated via three different network reconstruction methods (model which integrates 'ground truth' data). The yellow curves show the mutual information between the node-level properties inferred using our latent network model, the red curves show the same measures inferred using the union of reported data, and the blue curves show the same measures inferred using the intersection of reported data. The y-axis of each sub-figure represents the correlation between the 'true' node-level metrics and the node-level metrics estimated with each reconstruction method, and the x-axis represents the value of the focal simulation parameter given in the subheading. For example, the x-axis in figure 28a represents the average false positive rate used when simulating the reported network data.

(a) Average false positive rate, $\in (0.001, \ldots, 0.05)$

(b) Standard deviation of false positive rate, $\in (0.001, \ldots, 2)$

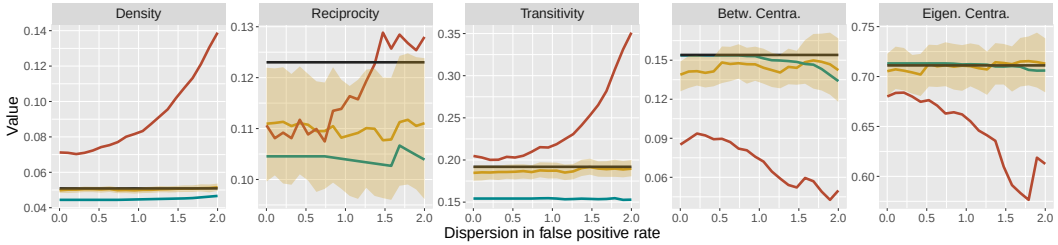

(c) Average recall of true tie rate, $\in (0.4, \ldots, 0.999)$

(d) Standard deviation of recall of true tie rate, $\in (0.001, \ldots, 2)$

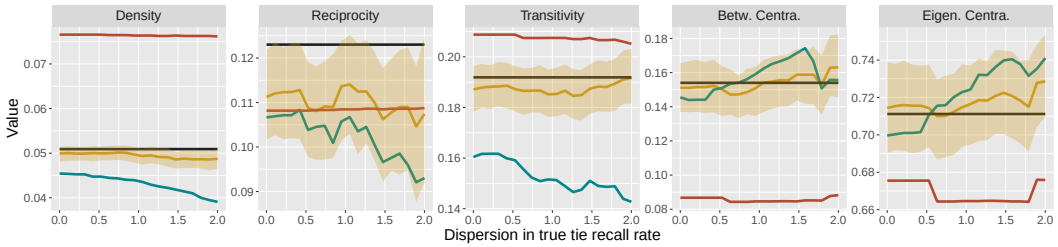

(e) Average false positive rate, $\in (0.001, \ldots, 0.02)$, and average recall of true tie rate, $\in (0.999, \ldots, 0.4)$

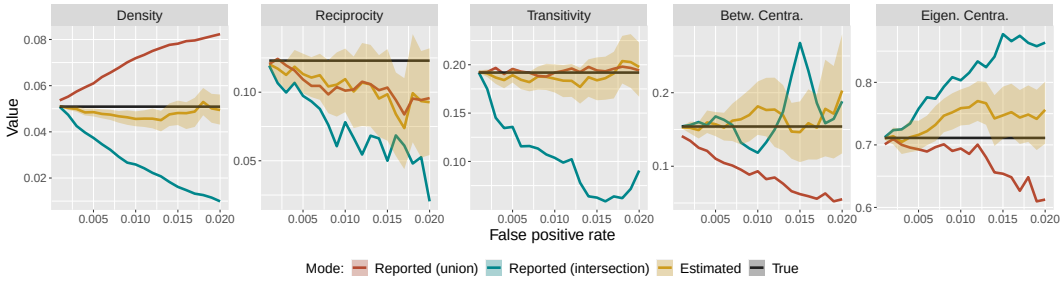

Fig. 29: Analysis of network-level properties (base model). The true network and all associated parameters are held fixed, except for the parameters displayed in the column labels, which range over the indicated support. The levels of each outcome in the true network appear as horizontal black lines. The yellow regions illustrate the posterior distributions of each outcome from the latent network model. The red and blue lines represent the outcomes resulting from application of either the union or intersection operator, respectively. The y-axis of each sub-figure represents the value of the indicated measures, and the x-axis represents the value of the focal simulation parameter given in the subheading. For example, the x-axis in figure 29a represents the average false positive rate used when simulating the reported network data.

(a) Average false positive rate, $\in (0.001, \ldots, 0.05)$

(b) Standard deviation of false positive rate, $\in (0.001, \ldots, 2)$

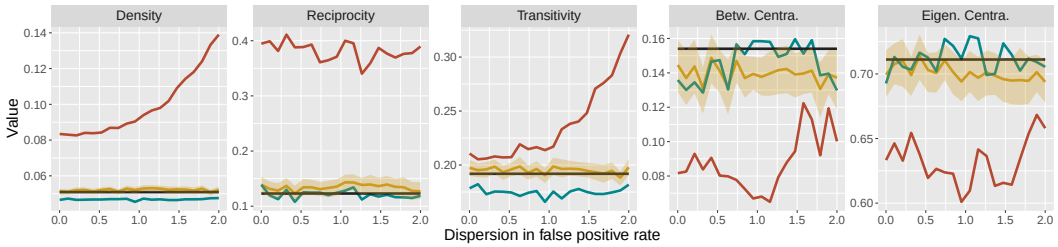

(c) Average recall of true tie rate, $\in (0.4, \ldots, 0.999)$

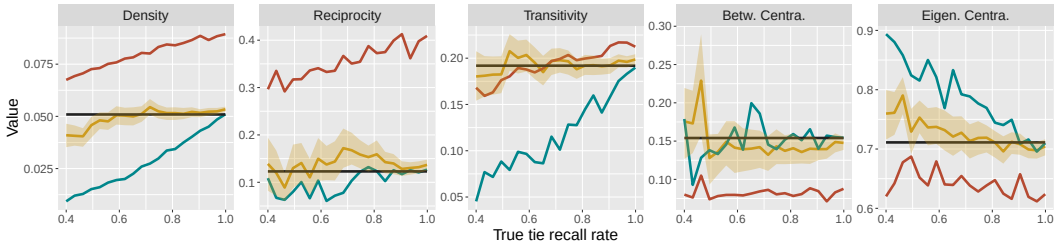

(d) Standard deviation of recall of true tie rate, $\in (0.001, \ldots, 2)$

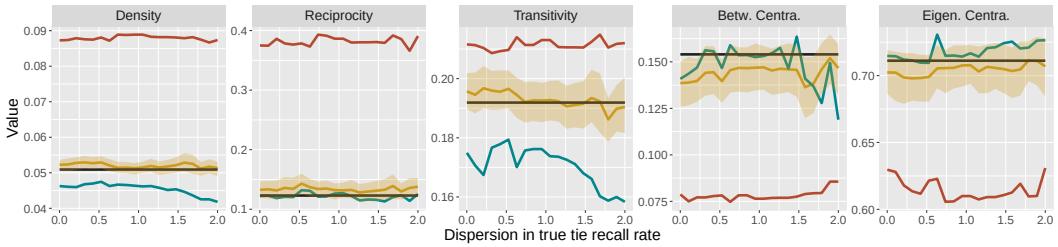

(e) Average false positive rate, $\in (0.001, \ldots, 0.02)$, and average recall of true tie rate, $\in (0.999, \ldots, 0.4)$

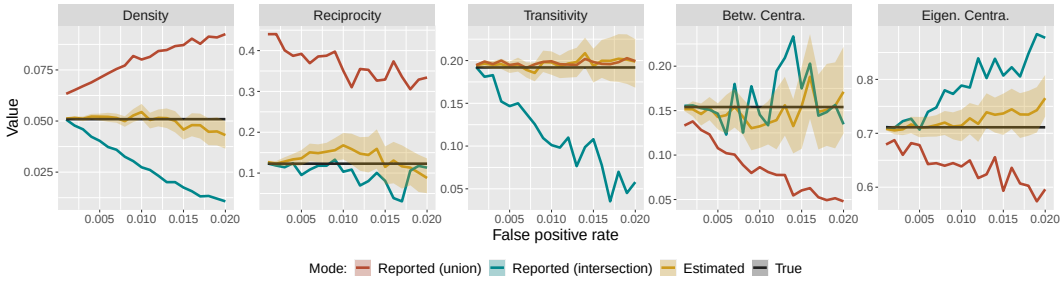

Fig. 30: Analysis of network-level properties (model with question order bias). The true network and all associated parameters are held fixed, except for the parameters displayed in the column labels, which range over the indicated support. The levels of each outcome in the true network appear as horizontal black lines. The yellow regions illustrate the posterior distributions of each outcome from the latent network model. The red and blue lines represent the outcomes resulting from application of either the union or intersection operator, respectively. The y-axis of each sub-figure represents the value of the indicated measures, and the x-axis represents the value of the focal simulation parameter given in the subheading. For example, the x-axis in figure 30a represents the average false positive rate used when simulating the reported network data.

(a) Average false positive rate, $\in (0.001, \ldots, 0.05)$

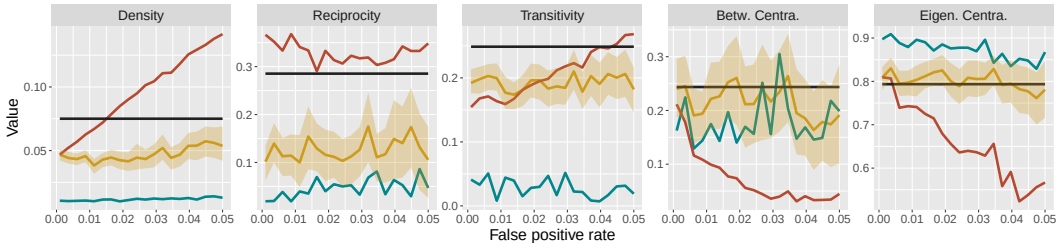

(b) Standard deviation of false positive rate, $\in (0.001, \ldots, 2)$

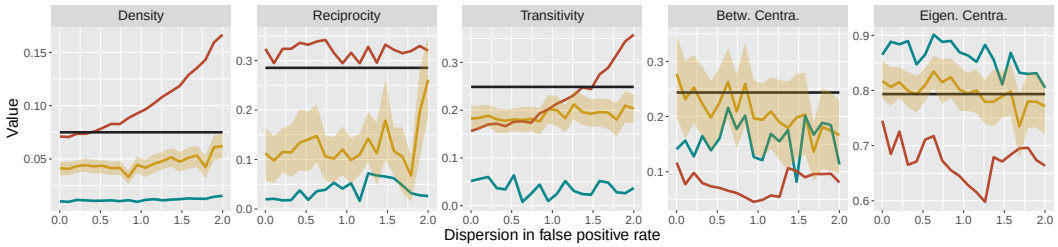

(c) Average recall of true tie rate, $\in (0.4, \ldots, 0.999)$

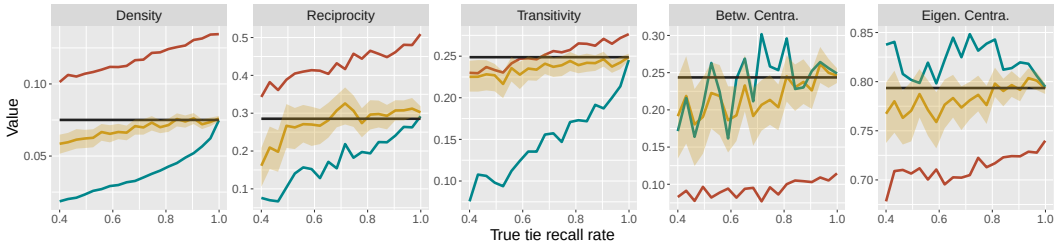

(d) Standard deviation of recall of true tie rate, $\in (0.001, \ldots, 2)$

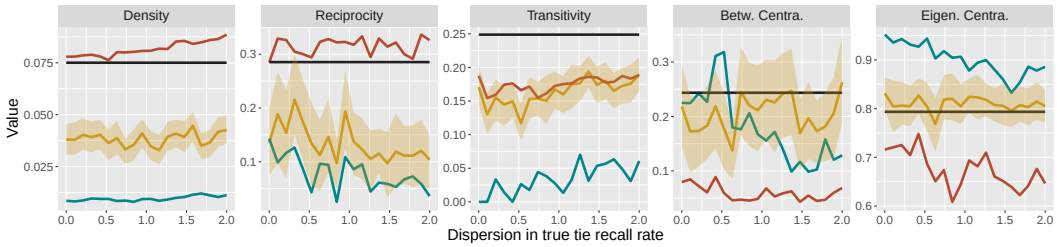

(e) Average false positive rate, $\in (0.001, \ldots, 0.02)$, and average recall of true tie rate, $\in (0.999, \ldots, 0.4)$

Fig. 31: Analysis of network-level properties (model with attribute-related bias). The true network and all associated parameters are held fixed, except for the parameters displayed in the column labels, which range over the indicated support. The levels of each outcome in the true network appear as horizontal black lines. The yellow regions illustrate the posterior distributions of each outcome from the latent network model. The red and blue lines represent the outcomes resulting from application of either the union or intersection operator, respectively. The y-axis of each sub-figure represents the value of the indicated measures, and the x-axis represents the value of the focal simulation parameter given in the subheading. For example, the x-axis in figure 31a represents the average false positive rate used when simulating the reported network data.

(a) Average false positive rate, $\in (0.001, \ldots, 0.05)$

(b) Standard deviation of false positive rate, $\in (0.001, \ldots, 2)$

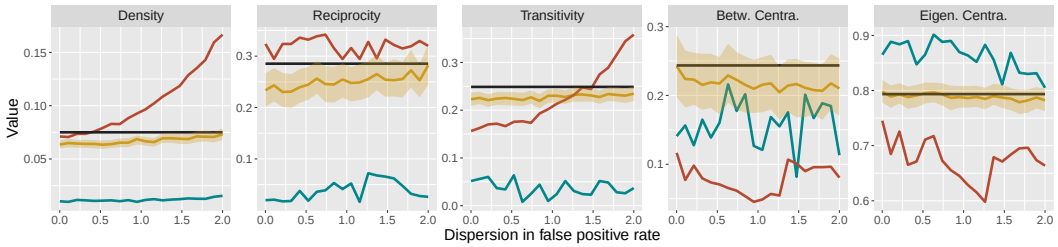

(c) Average recall of true tie rate, $\in (0.4, \ldots, 0.999)$

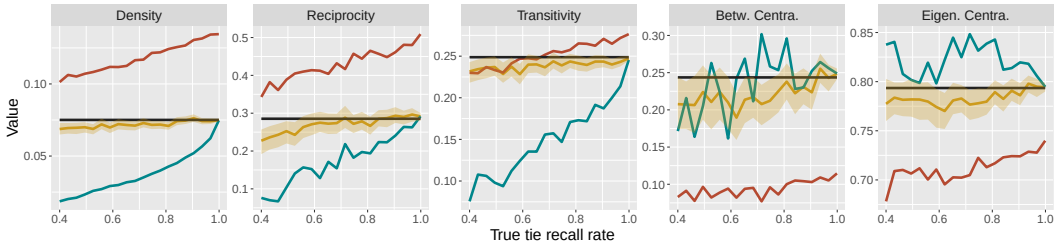

(d) Standard deviation of recall of true tie rate, $\in (0.001, \ldots, 2)$

(e) Average false positive rate, $\in (0.001, \ldots, 0.02)$, and average recall of true tie rate, $\in (0.999, \ldots, 0.4)$

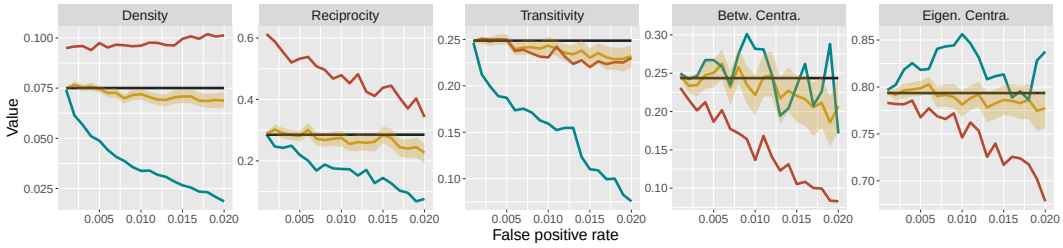

Fig. 32: Analysis of network-level properties (from the model that integrates 'ground truth' data). The true network and all associated parameters are held fixed, except for the parameters displayed in the column labels, which range over the indicated support. The levels of each outcome in the true network appear as horizontal black lines. The yellow regions illustrate the posterior distributions of each outcome from the latent network model. The red and blue lines represent the outcomes resulting from application of either the union or intersection operator, respectively. The y-axis of each sub-figure represents the value of the indicated measures, and the x-axis represents the value of the focal simulation parameter given in the subheading. For example, the x-axis in figure 32a represents the average false positive rate used when simulating the reported network data.

(a) Average false positive rate, $\in (0.001, \ldots, 0.05)$

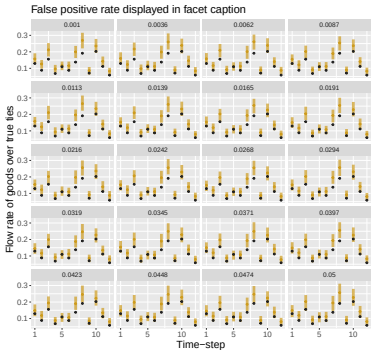

(b) Standard deviation of false positive rate, $\in (0.001, \ldots, 2)$

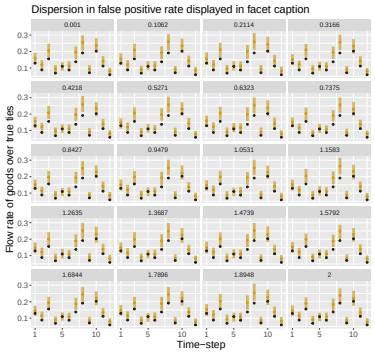

(c) Average recall of true tie rate, $\in (0.4, \ldots, 0.999)$

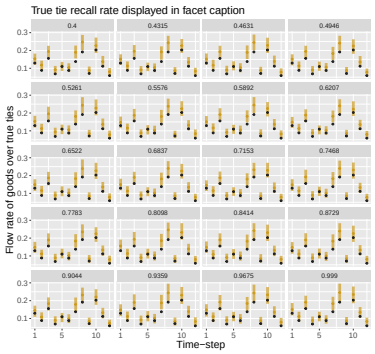

(d) Standard deviation of recall of true tie rate, $\in (0.001, \ldots, 2)$

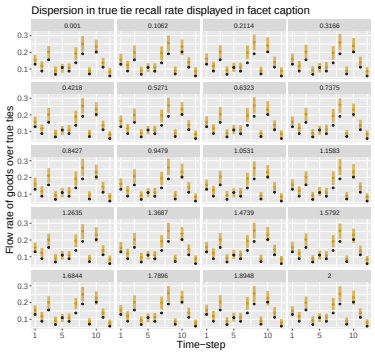

(e) Average false positive rate, $\in (0.001, \ldots, 0.02)$, and average recall of true tie rate, $\in (0.999, \ldots, 0.4)$

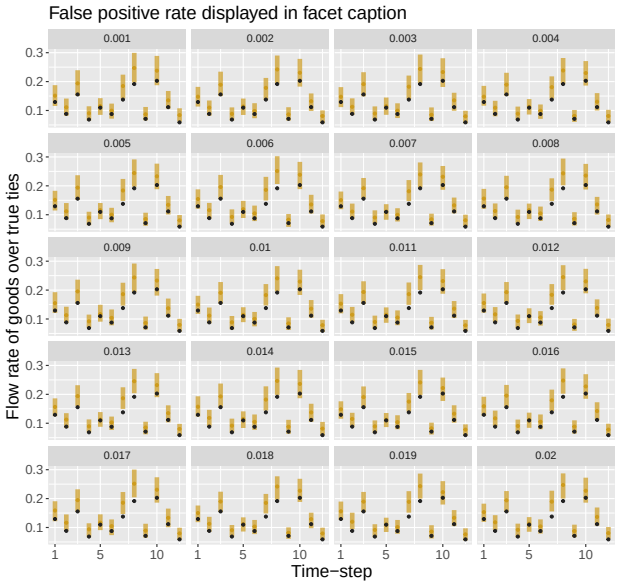

Fig. 33: Analysis of the rate at which transfers flow across 'true' ties in any given time-step (from the model that integrates 'ground truth' data). The true network at any given time-step, and all associated parameters, are held fixed—except for the parameters displayed in the facet captions. The true flow rates at each time-step are plotted as black points. The yellow regions display the posterior distributions of the flow rate at each time-step as recovered by the latent network model.

(a) Average false positive rate, $\in (0.001, \ldots, 0.05)$

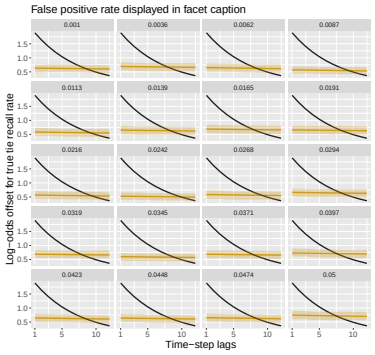

(b) Standard deviation of false positive rate, $\in (0.001, \ldots, 2)$

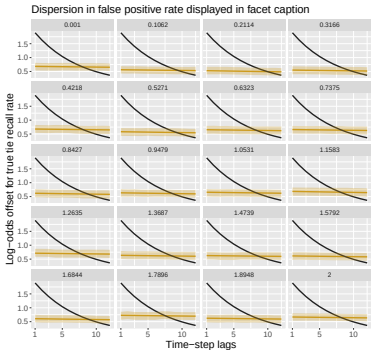

(c) Average recall of true tie rate, $\in (0.4, \ldots, 0.999)$

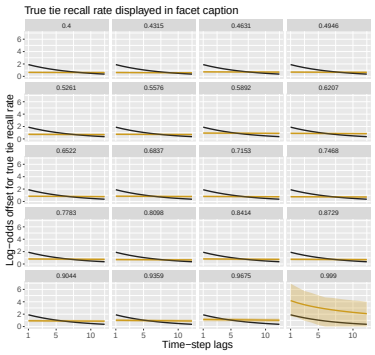

(d) Standard deviation of recall of true tie rate, $\in (0.001, \ldots, 2)$

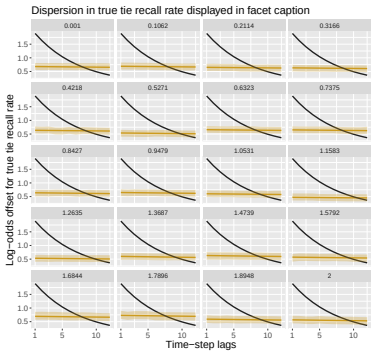

(e) Average false positive rate, $\in (0.001, \ldots, 0.02)$, and average recall of true tie rate, $\in (0.999, \ldots, 0.4)$

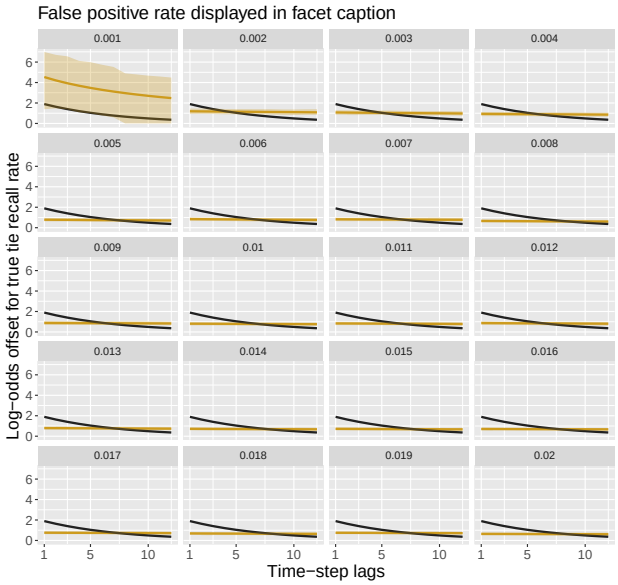

Fig. 34: The effect of true transfers on recall of ties (model which integrates 'ground truth' data). The true network and all associated parameters are held fixed. The generative values of the parameters appear as black lines. The yellow regions illustrate the posterior distributions of each parameter. The y axis illustrates how much the log-odds of recalling a true tie is impacted by a true transfer at a given time point. The x axis shows how many time steps in the past a transfer was observed.